Pergamon

Int. J. Solids Structures Vol. 33, No. 27, pp. 4019–4049, 1996

0020-7683/96 $15.00 + .00

0020-7683(95)00228-6

ELASTIC FIELD FOR ECCENTRICALLY LOADED RIGID PLATE ON MULTILAYERED SOLIDS

ZHONG QI YUE
Infrastructure Laboratory, Institute for Research in Construction,
National Research Council of Canada, Ottawa, Ontario, Canada K1A 0R6

(*Received* 23 *December* 1994; *in revised form* 11 *September* 1995)

Abstract—This paper presents an analytical investigation of the contact problem of a multilayered elastic solid subjected to the eccentric indentation of a rigid circular plate in the framework of classical elasticity. The total number of the dissimilar layers is an arbitrary integer n. These elastic layers can rest either on a dissimilar elastic halfspace or on a rigid rock base. The rigid circular plate is in smooth contact with the multilayered elastic solid. The classical theory of Fourier integral transforms is employed to solve the partial differential equations governing the behaviour of the multilayered elastic solid subjected to surface loading. Systems of standard Fredholm integral equations of the second-kind are then developed to govern the interaction between the rigid plate and the multilayered elastic solid. Explicit solution expression is further presented for the elastic field in the multilayered solid due to the eccentric indentation of the rigid plate. Closed-form results are respectively obtained for the singular stress field at the rigid plate edge in the multilayered elastic solid and for the elastic field in a homogeneous elastic halfspace induced by the eccentric indentation of the rigid plate. In particular, an asymptotic technique is utilized to overcome the difficulty associated with the convergence and singularity of the solution near or at the surface of the multilayered solid. Numerical results are presented to verify the techniques adopted in the paper and to illustrate the effect of layering material non-homogeneity on the elastic field induced by the eccentrically loaded rigid plate. The solution can be applied to the interpretation of non-destructive testing of layered materials such as highway and airport pavements. Crown Copyright © 1996 Published by Elsevier Science Ltd

1. INTRODUCTION

The main motivation of the present study originates from application of the solution to non-destructive evaluation of layered materials such as multilayered asphalt pavements. One of the most widely used non-destructive evaluation techniques of pavements is the Falling Weight Deflectometer (FWD) (Bush and Baladi, 1989; Monismith, 1992; May and Quintus, 1994). In a FWD device, a thick circular steel plate, either padded or not padded with thin rubber, is placed on the surface of a pavement and a pulse load is applied to the circular rigid plate by a falling weight through a resilient system. The effective moduli of the existing pavement structural layers are estimated by matching the measured maximum surface deflections at several sensor locations via a backcalculation procedure. A majority of the current backcalculation procedures are based on the multilayered elastic theory of pavements originally developed by Burminster (1945). In these backcalculation procedures, it was assumed that the contact pressure between the FWD loading plate and a multilayered pavement is uniformly distributed over a circular area (Mahoney *et al.*, 1989; May and Quintus, 1994). This oversimplified model of the contact pressure has a significant effect on the theoretical deflections in the near plate region and consequently induce errors in the backcalculated effective moduli of the pavement structural layers (Boddapati and Nazarian, 1993).

The objective of the present study is to present an analytical solution for the elastic response of a multilayered solid due to the eccentric indentation of a rigid plate. This analytical solution can be further used to improve backcalculation procedures for the non-destructive pavement evaluation using a FWD. Classical study of the relevant contact problems was given by Boussinesq (1885) using potential theory for a circular rigid plate smoothly in contact with a homogeneous elastic halfspace. This contact problem was re-examined by Sneddon and Harding (1945) and Sneddon (1946) for an explicit expression

of the induced elastic field using integral transform techniques. Since these classical works, studies related to contact problems of a plate-solid model have been extended to cover (i) flexibility of the plate; (ii) influence of plate geometry; (iii) interaction with external forces; (iv) influence of material anisotropy and plasticity; (v) dynamic loads and wave propagation effects; (vi) effect of frictional or rough contact; (vii) effect of saturated porous elastic media; (viii) influence of material heterogeneity. The literature on contact problems associated with a homogeneous elastic solid of either halfspace extent or layer extent have been well documented by a number of authors including Uflyand (1968), Poulos and Davis (1974), de Pater and Kalker (1975), Selvadurai (1979), Gladwell (1980), Fabrikant (1989), Yue and Selvadurai (1994), and Selvadurai and Yue (1994). The following is a brief review of previous studies available in the relevant literature of contact problems associated with multilayered or non-homogeneous elastic solids.

Schiffman (1962) presented a general theoretical study of stresses and displacements in multilayered elastic systems subjected to surface loading and developed systems of dual integral equations governing the indentation of a smooth circular rigid plate. Wu and Chiu (1967) considered the plane strain problem in an one-layered elastic halfplane and reduced the mixed boundary value problem to a single Fredholm integral equation of the second kind. Dhaliwa (1970) was able to reduce the axisymmetric problem of a flat ended cylindrical punch on an one-layered elastic halfspace to a Fredholm integral equation of the second kind which he solved approximately. Carrier and Christian (1973) analyzed the axisymmetric displacements and stresses in a linearly non-homogeneous halfspace induced by a rigid circular plate using a finite element technique. Chen and Engel (1974) used a least-squares approach to solve the axisymmetric contact problem, and presented the pressure profile under indenters of various geometries for a two-layered elastic halfspace. Rowe and Booker (1981) examined the axisymmetric surface settlement of a non-homogeneous elastic soil with a crust subjected to a rigid circular footing using a finite layer analysis method. Booker *et al.* (1985) provided analytical solutions for the behaviour of a smooth rigid disc due to a normal load or a moment on the surface of a non-homogeneous halfspace in which the Young's modulus E varies with the depth z as $E = M_E z^{\delta}$ $(0 \leqslant \delta \leqslant 1)$. Chow (1987) suggested a method, based on an axisymmetric finite element analysis, for effectively estimating the vertical displacements of rigid flat foundations of arbitrary shape on layered elastic soils. King (1987) examined the contact problems of flat-ended cylindrical, quadrilateral, and triangular punches indenting a one-layered elastic halfspace using a basis function technique (for the former two) and a singular integral equation for the latter. The load-deflection relation provided a basis for the estimation of Young's modulus of thin films for initial unloading compliance observed in indentation tests. Rajapakse and Selvadurai (1991), using a variational technique, further examined the axisymmetric response of a circular footing and an anchor plate in a linearly non-homogeneous elastic soil of halfspace extent. Gao *et al.* (1992) considered the problem of a rigid cylindrical punch indenting a one- or two-layered elastic halfspace using a moduli-perturbation method and used the first-order approximated solution to model the unloading phase of a micro-indentation test of the thin films deposited on a substrate. An axisymmetric finite element analysis was also performed to investigate the effects of a penny-shaped debonding crack along the film/substrate interface on the unloading compliance, and to analyze the energy release rate of the crack.

The present paper in particular extends the analytical investigation to cover the contact problem of a multilayered elastic solid subjected to the eccentric indentation of a rigid circular plate (Fig. 1) in the framework of classical elasticity. The total number of the dissimilar layers is an arbitrary integer n. These dissimilar homogeneous elastic layers can rest on either a dissimilar elastic halfspace or a rigid rock base. The rigid circular plate is in smooth contact with the multilayered elastic solid. The classical theory of Fourier integral transforms is employed to solve the partial differential equations governing the behaviour of the multilayered elastic system subjected to surface loading. Systems of standard Fredholm integral equations of the second-kind are then developed to govern the interaction between the rigid plate and the multilayered elastic solid. Explicit solution expression is further presented for the elastic field in the multilayered solid due to the eccentric indentation of

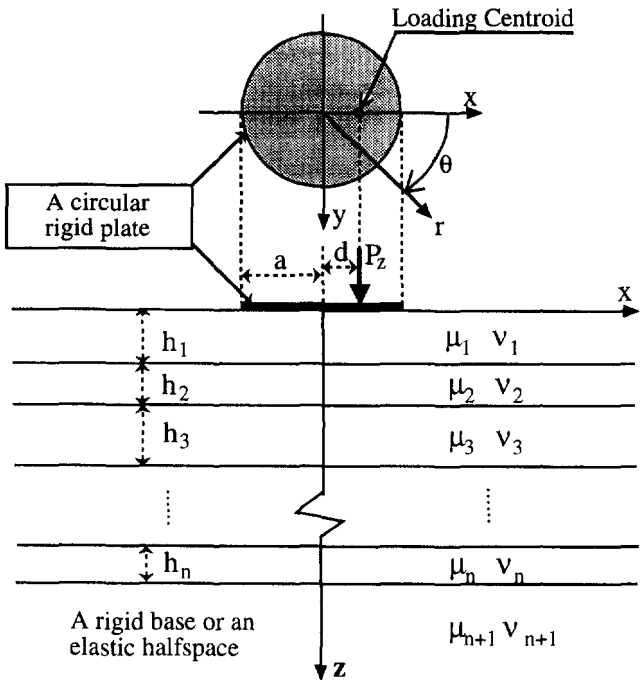

Fig. 1. A multilayered elastic solid eccentrically indented by a rigid plate.

the rigid plate. Closed-form results are respectively obtained for the singular stress field at the rigid plate edge in the multilayered elastic solid and for the elastic field in a homogeneous elastic halfspace induced by the eccentric indentation of the rigid plate. A computer program was developed to calculate the displacements, stresses, and strains in the multilayered elastic system induced by the eccentrically loaded rigid plate. In particular, an asymptotic technique was utilized to overcome the difficulty associated with the convergence and singularity of the solution near or at the surface of the multilayered solid. Numerical results are presented to verify the numerical techniques adopted in the paper and to illustrate the effect of layering material non-homogeneity on the elastic field induced by the eccentrically loaded rigid plate.

2. GOVERNING EQUATIONS

A brief account of the governing equations can be presented as follows in a Cartesian tensor notation. The constitutive equation governing the linear relations between stresses (σ_{ij}) and strains (ε_{ij}) in an isotropic solid takes the form

$$\sigma_{ij} = \frac{2\mu\nu}{1-2\nu}\varepsilon_{kk}\delta_{ij} + 2\mu\varepsilon_{ij}. \tag{1}$$

The strains are related to the displacements (u_i) by

$$\varepsilon_{ij} = \tfrac{1}{2}(u_{i,j} + u_{j,i}). \tag{2}$$

The governing equations are complete with the specification of equations of static equilibrium.

$$\sigma_{ij,j} = 0 \tag{3}$$

where δ_{ij} is the Kronecker delta; $i, j = x, y$, or z; μ and ν are, respectively, shear modulus and Poisson's ratio characterizing an isotropic elastic solid.

Based on the classical theory of Fourier integral transforms (Sneddon, 1972), it can be shown that the following set of solution representations exists for the field variables in an elastic layer ($0 \leqslant r < +\infty$, $0 \leqslant \theta < 2\pi$, $a \leqslant z \leqslant b$) in the cylindrical coordinate systems ($Or\theta z$ and $O\rho\varphi z$) (Yue, 1988; Yue and Wang, 1988; Yue, 1992; Yue, 1995).

$$\mathbf{u}(r,\theta,z) = \frac{1}{2\pi}\int_0^{\infty}\int_0^{2\pi} \Pi\mathbf{w}(\rho,\varphi,z)K\,\mathrm{d}\varphi\,\mathrm{d}\rho$$

$$\mathbf{w}(\rho,\varphi,z) = \frac{\rho}{2\pi}\int_0^{\infty}\int_0^{2\pi} \Pi^*\mathbf{u}(r,\theta,z)K^*r\,\mathrm{d}\theta\,\mathrm{d}r$$

$$\mathbf{T}_z(r,\theta,z) = \frac{1}{2\pi}\int_0^{\infty}\int_0^{2\pi} \Pi\mathbf{Y}_z(\rho,\varphi,z)K\rho\,\mathrm{d}\varphi\,\mathrm{d}\rho$$

$$\mathbf{Y}_z(\rho,\varphi,z) = \frac{1}{2\pi}\int_0^{\infty}\int_0^{2\pi} \Pi^*\mathbf{T}_z(r,\theta,z)K^*r\,\mathrm{d}\theta\,\mathrm{d}r$$

$$\Gamma_p(r,\theta,z) = \frac{1}{2\pi}\int_0^{\infty}\int_0^{2\pi} \Pi_p\mathbf{w}(\rho,\varphi,z)K\rho\,\mathrm{d}\varphi\,\mathrm{d}\rho \tag{4}$$

where the integration areas of the two-dimensional (2-D) integral are the two horizontal planes (S and $\tilde{S}$) in the physical and transform domains, respectively. These integrals are in the sense of the Cauchy principal values. The vector fields in eqns (4) are defined by $\mathbf{u} = [u_r, u_\theta, u_z]^T$, $\mathbf{T}_z = [\sigma_{rz}, \sigma_{\theta z}, \sigma_{zz}]^T$, $\Gamma_p = [\varepsilon_{rr}, \varepsilon_{r\theta}, \varepsilon_{\theta\theta}]^T$; $\mathbf{w} = [w_1, w_2, w_3]^T$, and $\mathbf{Y}_z = [\tau_1, \tau_2, \tau_3]^T$; where the superscript T stands for the transpose of matrix. $\mathbf{w}$ and $\mathbf{Y}_z$ are two vectors in the transform domain. K^* and Π^* are, respectively, the complex conjugates of the Fourier matrix kernel functions $K(=\mathrm{e}^{ir\sin(\theta-\varphi)}, i=\sqrt{-1})$ and Π defined by

$$\Pi = \begin{pmatrix} i\sin(\theta+\varphi) & i\cos(\theta+\varphi) & 0 \\ i\cos(\theta+\varphi) & -i\sin(\theta+\varphi) & 0 \\ 0 & 0 & 1 \end{pmatrix}$$

$$\Pi_p = -\frac{1}{2}\begin{pmatrix} 1-\cos 2(\theta+\varphi) & \sin 2(\theta+\varphi) & 0 \\ \sin 2(\theta+\varphi) & \cos 2(\theta+\varphi) & 0 \\ 1+\cos 2(\theta+\varphi) & -\sin 2(\theta+\varphi) & 0 \end{pmatrix}. \tag{5}$$

The relationships between the Cartesian and cylindrical coordinates are defined by $x = r\cos\theta$ and $y = r\sin\theta$. In the following, we shall note that $\mathbf{w}(z) = \mathbf{w}(\rho,\varphi,z)$, and $\mathbf{Y}_z(z) = \mathbf{Y}_z(\rho,\varphi,z)$ for simplicity.

The partial differential eqns (1–3) governing the behaviour of an elastic layer can then be reduced to the following two sets of first-order ordinary differential equations in terms of the two vectors in the Fourier transform domain. i.e.,

$$\frac{\mathrm{d}}{\mathrm{d}z}\mathbf{V}(z) = \rho\mathbf{C}_v\mathbf{V}(z)$$

$$\frac{\mathrm{d}}{\mathrm{d}z}\mathbf{U}(z) = \rho\mathbf{C}_u\mathbf{U}(z) \tag{6}$$

where $\mathbf{V} = [w_2, \tau_2]^T$, $\mathbf{U} = [w_1, w_3, \tau_3, \tau_1]^T$, and

$$\mathbf{C}_v = \begin{pmatrix} 0 & \dfrac{1}{\mu} \\ \mu & 0 \end{pmatrix}, \quad \mathbf{C}_u = \begin{bmatrix} 0 & -1 & 0 & \dfrac{1}{\mu} \\ 1-2\alpha & 0 & \dfrac{\alpha}{\mu} & 0 \\ 0 & 0 & 0 & 1 \\ 4\mu(1-\alpha) & 0 & 2\alpha-1 & 0 \end{bmatrix}, \quad \alpha = \frac{1-2\nu}{2(1-\nu)}. \tag{7}$$

By solving these linear systems of ordinary differential equations, we obtain the following algebraic equations governing the field variables in the transform domain.

$$\begin{aligned} \mathbf{V}(z) &= \mathrm{e}^{\rho(b-z)}\mathbf{A}(b-z)\mathbf{V}(b) \\ \mathbf{U}(z) &= \mathrm{e}^{\rho(b-z)}\mathbf{Q}(b-z)\mathbf{U}(b) \end{aligned} \tag{8}$$

where $z \leqslant b$, and the fundamental matrices $\mathbf{A}(\chi)$ and $\mathbf{Q}(\chi)$ are defined by

$$\begin{aligned} \mathbf{A}(\chi) &= \tfrac{1}{2}[\mathbf{A}_q + \mathrm{e}^{-2\rho\chi}\mathbf{A}_p] \\ \mathbf{Q}(\chi) &= \tfrac{1}{2}[\mathbf{Q}_q - \rho\chi\mathbf{R}_q + \mathrm{e}^{-2\rho\chi}[\mathbf{Q}_p - \rho\chi\mathbf{R}_p]]. \end{aligned} \tag{9}$$

The algebraic governing equations for an elastic halfspace ($b \leqslant z < \infty$) can be further simplified as follows using the natural regularity boundary conditions as $z \to \infty$,

$$\begin{aligned} 2\mathbf{V}(z) &= \mathrm{e}^{-\rho(z-b)}\mathbf{A}_q\mathbf{V}(b) \\ 2\mathbf{U}(z) &= \mathrm{e}^{-\rho(z-b)}[\mathbf{Q}_q + \rho(z-b)\mathbf{R}_q]\mathbf{U}(b). \end{aligned} \tag{10}$$

In eqns (9, 10), $\mathbf{A}_p$, $\mathbf{A}_q$, $\mathbf{Q}_p$, $\mathbf{Q}_q$, $\mathbf{R}_p$, and $\mathbf{R}_q$ are six constant square matrices defined by

$$\mathbf{A}_p = \begin{pmatrix} 1 & \dfrac{1}{\mu} \\ \mu & 1 \end{pmatrix}, \quad \mathbf{A}_q = \begin{pmatrix} 1 & -\dfrac{1}{\mu} \\ -\mu & 1 \end{pmatrix}$$

$$\mathbf{Q}_p = \begin{bmatrix} 1 & -\alpha & 0 & \dfrac{1+\alpha}{2\mu} \\ -\alpha & 1 & \dfrac{1+\alpha}{2\mu} & 0 \\ 0 & 2\mu[1-\alpha] & 1 & \alpha \\ 2\mu[1-\alpha] & 0 & \alpha & 1 \end{bmatrix}$$

$$\mathbf{Q}_q = \begin{bmatrix} 1 & \alpha & 0 & -\dfrac{1+\alpha}{2\mu} \\ \alpha & 1 & -\dfrac{1+\alpha}{2\mu} & 0 \\ 0 & 2\mu[\alpha-1] & 1 & -\alpha \\ 2\mu[\alpha-1] & 0 & -\alpha & 1 \end{bmatrix}$$

$$\mathbf{R}_p = (1-\alpha)\begin{bmatrix} 1 & -1 & -\frac{1}{2\mu} & \frac{1}{2\mu} \\ 1 & -1 & -\frac{1}{2\mu} & \frac{1}{2\mu} \\ 2\mu & -2\mu & -1 & 1 \\ 2\mu & -2\mu & -1 & 1 \end{bmatrix}$$

$$\mathbf{R}_q = (1-\alpha)\begin{bmatrix} -1 & -1 & \frac{1}{2\mu} & \frac{1}{2\mu} \\ 1 & 1 & -\frac{1}{2\mu} & -\frac{1}{2\mu} \\ -2\mu & -2\mu & 1 & 1 \\ 2\mu & 2\mu & -1 & -1 \end{bmatrix}. \tag{11}$$

3. THE MIXED BOUNDARY VALUE PROBLEM

The mixed boundary value problem considered here is a multilayered elastic solid subjected to the eccentric indentation of a rigid circular and smooth plate (see Fig. 1). The multilayered elastic solid consists of n dissimilar elastic layers which are either adhering to an elastic halfspace or lying in smooth or rough contact with a rigid base. Referring to the cylindrical coordinates in Fig. 1, it can be noted that the j-th elastic layer occupies a layer region of $H_{j-1}^{+} \leqslant z \leqslant H_j^{-}$ and has the thickness $h_j (= H_j - H_{j-1})$, the shear modulus μ_j and the Poisson's ratio ν_j ($j = 1, 2, 3, \ldots, n$ and $H_0 = 0$). The $(n+1)$-th layer can be either a rigid rock base of an elastic solid which occupies a halfspace region ($H_n^{+} \leqslant z < +\infty$) and has the shear modulus μ_{n+1} and the Poisson's ratio ν_{n+1}. For the perfectly bonded interface connection, the vertical stress vector $\mathbf{T}_z(r, \theta, z)$ and the displacement vector $\mathbf{u}(r, \theta, z)$ are completely continuous at the horizontal interface between any two connected dissimilar elastic layers, i.e.,

$$\lim_{z \to H_j^{-}} \mathbf{T}_z(r, \theta, z) = \mathbf{T}_z(r, \theta, H_j), \quad \lim_{z \to H_j^{+}} \mathbf{u}(r, \theta, z) = \mathbf{u}(r, \theta, H_j); \quad j = 1, 2, \ldots, n. \tag{12}$$

The mixed boundary conditions at the surface ($z = H_0 = 0$) of the multilayered elastic solid can be written as follows,

$$\begin{aligned} &\sigma_{zz}(r, \theta, 0) = 0, \quad a < r < \infty, \quad 0 \leqslant \theta < 2\pi \\ &u_z(r, \theta, 0) = D_z + \Omega_y r \cos\theta, \quad 0 \leqslant r < a, \quad 0 \leqslant \theta < 2\pi \end{aligned} \tag{13}$$

where a is the radius of the rigid circular plate; D_z is the axial translation of the rigid plate along the z-axis and Ω_y is the central rotation of the rigid plate about the y-axis. The shear stresses at the entire surface ($z = 0$) are zero, i.e., $\sigma_{rz}(r, \theta, 0) = 0$ and $\sigma_{\theta z}(r, \theta, 0) = 0$, where $0 \leqslant r < \infty$ and $0 \leqslant \theta < 2\pi$. The axial load P_z and its associated moment $M_y (= P_z d)$ acting on the rigid plate have the following integral relations withe the contact normal stress $\sigma_{zz}(r, \theta, 0)$.

$$\begin{aligned} P_z &= -\int_0^a \int_0^{2\pi} \sigma_{zz}(r, \theta, 0) r \, \mathrm{d}\theta \, \mathrm{d}r \\ M_y &= P_z d = -\int_0^a \int_0^{2\pi} \sigma_{zz}(r, \theta, 0) r^2 \cos\theta \, \mathrm{d}\theta \, \mathrm{d}r \end{aligned} \tag{14}$$

where d is the eccentricity of the external load P_z acting on the rigid circular plate.

4. SOLUTION IN THE TRANSFORM DOMAIN

Using the governing eqns (8)–(11) and the boundary and interfacial conditions (12)–(13), it can be shown that $\mathbf{w}(z)$ and $\mathbf{Y}_z(z)$ have the following expression.

$$\mathbf{w}(z) = \frac{1}{\mu_1}\Phi(\rho, z)\tau_3(\rho, \varphi, 0), \quad \mathbf{Y}_z(z) = \Psi(\rho, z)\tau_3(\rho, \varphi, 0) \tag{15}$$

where $\tau_3(\rho, \varphi, 0)$ is the unknown contact normal stress in the transform domain. The kernel functions $\Phi(\rho, z) = [\Phi_{13}, 0, \Phi_{33}]^T$ and $\Psi(\rho, z) = [\Psi_{13}, 0, \Psi_{33}]^T$ are specifically given in the following using the backward transfer matrix technique (Yue and Wang, 1988; Yue, 1995).

$$\left[\frac{1}{\mu_1}\Phi_{13}, \frac{1}{\mu_1}\Phi_{33}, \Psi_{33}, \Psi_{13}\right]^T = e^{-\rho z}\Phi_u(\rho, z)\Gamma_u(\rho) \tag{16}$$

where

$$\Phi_u(\rho, z) = \begin{cases} \mathbf{Q}_j(z - H_j), & H_{j-1} \leqslant z \leqslant H_j \\ \frac{1}{2}[\mathbf{Q}_{q(n+1)} + \rho(z - H_n)\mathbf{R}_{q(n+1)}], & z \geqslant H_n \end{cases}$$

$$\Gamma_u(\rho) = \begin{cases} \mathbf{Q}_{j-1}(h_{j+1})\mathbf{Q}_{j+2}(h_{j-2}) \ldots \mathbf{Q}_n(h_n)\mathbf{M}_u^{-1}(\rho)\mathbf{I}_u, & H_{j-1} \leqslant z \leqslant H_j \\ \mathbf{M}_u^{-1}(\rho)\mathbf{I}_u, & z \geqslant H_n \end{cases} \tag{17}$$

where $j = 1, 2, 3, \ldots, n$. $\mathbf{I}_u = [0, 0, 1, 0]^T$. $\mathbf{M}_u^{-1}(\rho)$ is the inverse matrix of the coefficient matrix $\mathbf{M}_u(\rho)$ defined in the following equations.

$$\mathbf{M}_u = \begin{pmatrix} \mathbf{P}_p \\ \mathbf{P}_q\mathbf{Q}_{1n} \end{pmatrix} \tag{18}$$

where $\mathbf{Q}_{1n} = \mathbf{Q}_1(h_1)\mathbf{Q}_2(h_2) \ldots \mathbf{Q}_n(h_n)$.

$$\mathbf{P}_q = \begin{pmatrix} 0 & 0 & 1 & 0 \\ 0 & 0 & 0 & 1 \end{pmatrix};$$

(i) if the $(n+1)$-th layer is an elastic halfspace,

$$\mathbf{P}_p = \begin{bmatrix} 1 & -1 & -\dfrac{1}{2\mu_{n+1}} & \dfrac{1}{2\mu_{n+1}} \\ 1 - \alpha_{n-1} & 1 - \alpha_{n+1} & \dfrac{1 + \alpha_{n+1}}{2\mu_{n-1}} & \dfrac{1 + \alpha_{n-1}}{2\mu_{n+1}} \end{bmatrix};$$

(ii) if the $(n+1)$-th layer is a rough rigid base,

$$\mathbf{P}_p = \begin{pmatrix} 1 & 0 & 0 & 0 \\ 0 & 1 & 0 & 0 \end{pmatrix};$$

or (iii) if the $(n+1)$-th layer is a smooth rigid base,

$$\mathbf{P}_p = \begin{pmatrix} 0 & 0 & 0 & 1 \\ 0 & 1 & 0 & 0 \end{pmatrix}.$$

The matrix $\mathbf{Q}_j(\chi)$ in the above equations is obtained from eqns (8–11) by substituting μ and α with μ_j and α_j, respectively.

5. GOVERNING INTEGRAL EQUATIONS

Using the eqns (4), (13) and (15), the following set of two-dimensional (2-D) integral equations can be obtained for the eccentric indentation of the smooth rigid plate (Yue, 1992; Yue and Selvadurai, 1994).

$$\frac{1}{2\pi}\int_0^{\infty}\int_0^{2\pi}[1+k_3]\tau_3(\rho,\varphi,0)K\,\mathrm{d}\varphi\,\mathrm{d}\rho=\frac{-\mu_1}{1-\nu_1}[D_z+\Omega_y r\cos\theta],\quad 0\leqslant r\leqslant a,\quad 0\leqslant\theta<2\pi$$

$$\frac{1}{2\pi}\int_0^{\infty}\int_0^{2\pi}\tau_3(\rho,\varphi,0)K\rho\,\mathrm{d}\varphi\,\mathrm{d}\rho=0,\quad a<r<\infty,\quad 0\leqslant\theta<2\pi, \tag{19}$$

where k_3 is a non-dimensional function of ρh_j, μ_j and ν_j $(j=1,2,3,\ldots,n+1)$ and is given by the following equation:

$$k_3=\frac{1}{(\nu_1-1)}\Phi_{33}(\rho,z)|_{z=0}-1. \tag{20}$$

The above 2-D integral equations can be decoupled into the following two sets of dual integral equations by using Fourier series expansions, where $\tau_3(\rho,\varphi,0)=\tau_{30}(\rho)-2i\sin\varphi\tau_{31}(\rho)$.

$$\int_0^{\infty}[1+k_3]\tau_{30}(\rho)J_0(\rho r)\,\mathrm{d}\rho=\frac{-\mu_1}{1-\nu_1}D_z,\quad 0\leqslant r\leqslant a$$

$$\int_0^{\infty}\tau_{30}(\rho)J_0(\rho r)\rho\,\mathrm{d}\rho=0,\quad a<r<\infty \tag{21}$$

and

$$\int_0^{\infty}[1+k_3]\tau_{31}(\rho)J_1(\rho r)\,\mathrm{d}\rho=\frac{-\mu_1}{1-\nu_1}\frac{r}{2}\Omega_y,\quad 0\leqslant r\leqslant a$$

$$\int_0^{\infty}\tau_{31}(\rho)J_1(\rho r)\rho\,\mathrm{d}\rho=0,\quad a<r<\infty. \tag{22}$$

The two sets of dual integral eqns (21) and (22) are singular integral equations with the regular singularity of $1/\sqrt{a^2-r^2}$. To isolate the singularity, the following solution representations are defined for $\tau_{30}(\rho)$ and $\tau_{31}(\rho)$ in terms of the auxiliary functions $\phi_0(x)$ and $\phi_1(x)$, respectively (Sneddon, 1972).

$$\tau_{30}(\rho)=\int_0^a\phi_0(x)\cos(\rho x)\,\mathrm{d}x$$

$$\tau_{31}(\rho)=\int_0^a\phi_1(x)\sin(\rho x)\,\mathrm{d}x. \tag{23}$$

The last equations in eqns (21) and (22) are then automatically satisfied. It is noted that

$$\int_0^{\infty}\tau_{30}(\rho)J_0(\rho r)\,\mathrm{d}\rho=\int_0^r\frac{\phi_0(x)}{\sqrt{r^2-x^2}}\mathrm{d}x$$

$$\int_0^{\infty}\tau_{31}(\rho)J_1(\rho r)\,\mathrm{d}\rho=\frac{1}{r}\int_0^r\frac{x\phi_1(x)}{\sqrt{r^2-x^2}}\mathrm{d}x. \tag{24}$$

Then the sets of dual integral equations can be reduced to the integral equation of the Abel type.

$$\int_0^r \frac{\phi_0(x)}{\sqrt{r^2-x^2}}\,dx+\int_0^\infty k_3\tau_{30}(\rho)J_0(\rho r)\,d\rho=\frac{-\mu_1}{1-\nu_1}D_z$$

$$\int_0^r \frac{x\phi_1(x)}{\sqrt{r^2-x^2}}\,dx+\int_0^\infty k_3\tau_{31}(\rho)rJ_1(\rho r)\,d\rho=\frac{-\mu_1}{1-\nu_1}\frac{r^2}{2}\Omega_y. \tag{25}$$

The solution of the Abel type integral eqns (25) can be written as the Fredholm integral equations of the second kind. For convenience, the following non-dimensional variables are introduced.

$$s=\frac{r}{a},\quad t=\frac{x}{a},\quad \phi_0(r)=-\frac{P_z}{2\pi a}\phi(s),\quad D_z=\frac{1-\nu_1}{4\mu_1 a}P_zX_z$$

$$b_j=\frac{h_j}{a},\quad \zeta=\frac{z}{a},\quad \phi_1(r)=-\frac{M_y}{4\pi a^2}\psi(s),\quad \Omega_y=\frac{1-\nu_1}{8\mu_1 a^3}M_yX_y. \tag{26}$$

The Fredholm integral equations of the second kind can then be reduced to the following non-dimensional forms.

$$\phi(s)+\int_0^1 K_0(s,t)\phi(t)\,dt=X_z$$

$$\psi(s)+\int_0^1 K_1(s,t)\psi(t)\,dt=sX_y \tag{27}$$

where $0\leqslant s\leqslant 1$, and the non-dimensional kernel functions are defined by the following semi-infinite integral,

$$K_0(s,t)=\frac{2}{\pi}\int_0^\infty k_3(\rho)\cos(\rho s)\cos(\rho t)\,d\rho$$

$$K_1(s,t)=\frac{2}{\pi}\int_0^\infty k_3(\rho)\sin(\rho s)\sin(\rho t)\,d\rho. \tag{28}$$

It can be shown that $|k_3|<B(1+\rho H_n/a)^2e^{-2\rho b_1}$, where B is a constant (Yue, 1995). As a result, the semi-infinite integral with the depending parameters s and t and the material parameters $(b_j, mu_j, nu_j; j=1,2,\ldots,n+1)$ in eqns (28) are uniformly and absolutely convergent integrals. The total axial load P_z and its associated moment M_y in eqns (14) can be evaluated by the following equations.

$$\int_0^1 \phi(t)\,dt=1,\quad \int_0^1 t\psi(t)\,dt=1. \tag{29}$$

It is noted that the systems of Fredholm integral equations of the second kind are standard and regular integral equations which can be accurately evaluated (Atkinson, 1976).

6. SOLUTION OF THE ELASTIC FIELD

The solution of the elastic field (i.e., displacements **u**, the vertical stresses $\mathbf{T}_z$ and the plane strains Γ_p) in the multilayered elastic solid induced by the eccentric indentation of

the rigid circular plate can be explicitly expressed as follows using the set of solution representations (4) and the solution of $\mathbf{w}(z)$ and $\mathbf{Y}_z(z)$ in eqns (15).

$$\mathbf{u}(s,\theta,\zeta)=\frac{-P_z}{2\pi a\mu_1}\left[\int_0^1\phi(t)\mathbf{K}_{uz}(s,\zeta,t)\,\mathrm{d}t+\frac{d}{2a}\Pi_a(\theta)\int_0^1\psi(t)\mathbf{K}_{uy}(s,\zeta,t)\,\mathrm{d}t\right]$$

$$\mathbf{T}_z(s,\theta,\zeta)=\frac{-P_z}{2\pi a^2}\left[\int_0^1\phi(t)\mathbf{K}_{zz}(s,\zeta,t)\,\mathrm{d}t+\frac{d}{2a}\Pi_a(\theta)\int_0^1\psi(t)\mathbf{K}_{zy}(s,\zeta,t)\,\mathrm{d}t\right]$$

$$\Gamma_p(s,\theta,\zeta)=\frac{-P_z}{4\pi a^2\mu_1}\left[\int_0^1\phi(t)\mathbf{K}_{pz}(s,\zeta,t)\,\mathrm{d}t+\frac{d}{2a}\Pi_a(\theta)\int_0^1\psi(t)\mathbf{K}_{py}(s,\zeta,t)\,\mathrm{d}t\right] \tag{30}$$

where $0\leqslant\zeta,\ s<\infty,\ 0\leqslant\theta<2\pi$. The kernel matrix functions are given in the following.

$$\mathbf{K}_{uz}=\begin{pmatrix}-K_c(\Phi_{13},1)\\0\\K_c(\Phi_{33},0)\end{pmatrix},\quad \mathbf{K}_{zz}=\begin{pmatrix}-K_c(\rho\Psi_{13},1)\\0\\K_c(\rho\Psi_{33},0)\end{pmatrix},\quad \Pi_a(\theta)=\begin{pmatrix}\cos\theta&0&0\\0&\sin\theta&0\\0&0&\cos\theta\end{pmatrix}$$

$$\mathbf{K}_{pz}=\begin{pmatrix}K_c(\rho\Phi_{13},2)-K_c(\rho\Phi_{13},0)\\0\\-K_c(\rho\Phi_{13},2)-K_c(\rho\Phi_{13},0)\end{pmatrix},\quad \mathbf{K}_{zy}=\begin{pmatrix}K_s(\rho\Psi_{13},0)-K_s(\rho\Psi_{13},2)\\-K_s(\rho\Psi_{13},0)-K_s(\rho\Psi_{13},2)\\2K_s(\rho\Psi_{33},1)\end{pmatrix}$$

$$\mathbf{K}_{uy}=\begin{pmatrix}K_s(\Phi_{13},0)-K_s(\Phi_{13},2)\\-K_s(\Phi_{13},0)-K_s(\Phi_{13},2)\\2K_s(\Phi_{33},1)\end{pmatrix},\quad \mathbf{K}_{py}=\begin{pmatrix}K_s(\rho\Phi_{13},3)-3K_s(\rho\Phi_{13},1)\\K_s(\rho\Phi_{13},3)+K_s(\rho\Phi_{13},1)\\-K_s(\rho\Phi_{13},3)-K_s(\rho\Phi_{13},1)\end{pmatrix}. \tag{31}$$

The functions $K_c(\Phi,m)$ and $K_s(\Phi,m)$ $(m=0,1,2,3)$ in eqns (31) are defined by the following semi-infinite integrals.

$$K_c(\Phi,m)=\int_0^\infty\Phi(\rho\zeta)J_m(\rho s)\cos(\rho t)\,\mathrm{d}\rho$$

$$K_s(\Phi,m)=\int_0^\infty\Phi(\rho\zeta)J_m(\rho s)\sin(\rho t)\,\mathrm{d}\rho. \tag{32}$$

In particular, at the surface of the multilayered elastic solid ($\zeta=0$), the solution can be further simplified as follows using eqns (16) to isolate the singular terms in the solution expression (30).

$$u_r(s,\theta,0)=\frac{(1-2\nu_1)P_z}{4\pi a\mu_1}\left[\int_0^1\phi(t)K_{u2}(s,t)\,\mathrm{d}t+\frac{d}{2a}\int_0^1\psi(t)K_{u3}(s,t)\,\mathrm{d}t\cos\theta\right]$$

$$u_\theta(s,\theta,0)=\frac{(1-2\nu_1)P_z}{4\pi a\mu_1}\left[\frac{d}{2a}\int_0^1\psi(t)K_{u4}(s,t)\,\mathrm{d}t\sin\theta\right]$$

$$u_z(s,\theta,0)=\begin{cases}\dfrac{(1-\nu_1)P_z}{4\mu_1 a}\left[X_z+\dfrac{sd}{2a}X_r\cos\theta\right], & 0\leqslant s\leqslant 1\\[2ex]\dfrac{(1-\nu_1)P_z}{2\pi\mu_1 a}\left[\displaystyle\int_0^1\phi(t)K_{u0}(s,t)\,\mathrm{d}t+\frac{d}{a}\int_0^1\psi(t)K_{u1}(s,t)\,\mathrm{d}t\cos\theta\right], & 1<s<\infty\end{cases}$$

$$\sigma_{zz}(s,\theta,0)=\frac{-P_z}{2\pi a^2}\left[G_1(s)+\frac{d}{a}G_2(s)\cos\theta\right]$$

$$\sigma_{rz}(s,\theta,0)=0$$

$$\sigma_{\theta z}(s,\theta,0)=0$$

$$\varepsilon_{rr}(s,\theta,0)=\frac{(1-2\nu_1)P_z}{8\pi a^2\mu_1}\left[\int_0^1\phi(t)K_{p0}(s,t)\,\mathrm{d}t+\frac{d}{2a}\int_0^1\psi(t)K_{p1}(s,t)\,\mathrm{d}t\cos\theta-2\left[G_1(s)+\frac{d}{a}G_2(s)\cos\theta\right]\right]$$

$$\varepsilon_{r\theta}(s,\theta,0)=\frac{(1-2\nu_1)P_z}{8\pi a^2\mu_1}\left[\frac{d}{2a}\int_0^1\psi(t)K_{p4}(s,t)\mathrm{d}t\sin\theta\right]$$

$$\varepsilon_{\theta\theta}(s,\theta,0)=\frac{(1-2\nu_1)P_z}{8\pi a^2\mu_1}\left[\int_0^1\phi(t)K_{p2}(s,t)\,\mathrm{d}t+\frac{d}{2a}\int_0^1\psi(t)K_{p3}(s,t)\,\mathrm{d}t\cos\theta\right]. \tag{33}$$

The kernel functions K_{um} and K_{pm} $(m=0,1,2,3,4)$ are given in the following.

$$K_{u0}(s,t)=\frac{1}{\sqrt{s^2-t^2}}+K_c(k_3,0)$$

$$K_{u1}(s,t)=\frac{t}{s\sqrt{s^2-t^2}}+K_s(k_3,1)$$

$$K_{u2}(s,t)=-F_3(s,t)-K_c(k_1,0)$$

$$K_{u3}(s,t)=2F_2(s,t)-\frac{2}{s}F_1(s,t)+K_s(k_1,0)-K_s(k_1,2)$$

$$K_{u4}(s,t)=-\frac{2}{s}F_1(s,t)-K_s(k_1,0)-K_s(k_1,2)$$

$$K_{p0}(s,t)=\frac{2}{s}F_3(s,t)+K_c(\rho k_1,2)-K_c(\rho k_1,0)$$

$$K_{p1}(s,t)=\frac{4}{s}\left[\frac{2}{s}F_1(s,t)-F_2(s,t)\right]+K_s(\rho k_1,3)-3K_s(\rho k_1,1)$$

$$K_{p2}(s,t)=-\frac{2}{s}F_3(s,t)-K_c(\rho k_1,2)-K_c(\rho k_1,0)$$

$$K_{p3}(s,t)=-\frac{4}{s}\left[\frac{2}{s}F_1(s,t)-F_2(s,t)\right]-K_s(\rho k_1,3)-3K_s(\rho k_1,1)$$

$$K_{p4}(s,t)=\frac{4}{s}\left[\frac{2}{s}F_1(s,t)-F_2(s,t)\right]+K_s(\rho k_1,3)+K_s(\rho k_1,1) \tag{34}$$

where k_3 is given by eqn (20) and $k_1=[2/(2\nu_1-1)]\Phi_{13}(\rho,z)|_{z=0}-1$. It also can be shown that $|k_1|<C(1+\rho H_n/a)^2\mathrm{e}^{-2\rho h_1}$, where C is constant. As a result, the semi-infinite integral with the depending parameters s and t and the material parameters $(b_j, mu_j, nu_j;\ j=1,2,\ldots,n+1)$ in eqns (34) are uniformly and absolutely convergent integrals.

The functions $F_m(s,t)$ $(m=1,2,3)$, $G_1(s)$ and $G_2(s)$ in eqns (34) are expressed exactly as follows.

$$F_1(s,t)=\begin{cases}\dfrac{t}{t+\sqrt{t^2-s^2}}, & s\leqslant t\\ \dfrac{t}{s}, & s\geqslant t\end{cases}$$

$$F_2(s,t)=\begin{cases}\dfrac{1}{\sqrt{t^2-s^2}}, & s<t\\ 0, & s\geqslant t\end{cases}$$

$$F_3(s,t)=\begin{cases}\dfrac{-s}{\sqrt{t^2-s^2}(t+\sqrt{t^2-s^2})}, & s<t\\ \dfrac{1}{s}, & s\geqslant t\end{cases}$$

$$G_1(s)=\begin{cases}\dfrac{\phi(1)}{\sqrt{1-s^2}}-\displaystyle\int_s^1\frac{\mathrm{d}\phi(t)}{\mathrm{d}t}\frac{\mathrm{d}t}{\sqrt{t^2-s^2}}, & 0\leqslant s<1\\ 0, & 1<s<\infty\end{cases}$$

$$G_2(s)=\begin{cases}\dfrac{s\psi(1)}{\sqrt{1-s^2}}-s\displaystyle\int_s^1\frac{\mathrm{d}}{\mathrm{d}t}\left(\frac{\psi(t)}{t}\right)\frac{\mathrm{d}t}{\sqrt{t^2-s^2}}, & 0\leqslant s<1\\ 0, & 1<s<\infty\end{cases}. \tag{35}$$

The two functions $G_1(s)$ and $G_2(s)$ govern the singularity of the contact stress and the strains at the surface ($\zeta=0$). Furthermore, solution of the plane stresses $\mathbf{T}_p=[\sigma_{rr},\sigma_{r\theta},\sigma_{\theta\theta}]^{\mathrm{T}}$ and the vertical strains $\Gamma_z=[\varepsilon_{rz},\varepsilon_{\theta z},\varepsilon_{zz}]^{\mathrm{T}}$ can be easily and uniquely calculated by using the solution of $\mathbf{T}_z$ and Γ_p and the constitutive relation (1).

7. ASYMPTOTIC STRESS FIELD NEAR THE PLATE EDGE

It is well known that the stress field in an elastic solid induced by the indentation of a rigid plate is singular at the edge of the rigid plate. In the ensuing, analytical results are given to illustrate the asymptotic behaviour of the elastic stress field near the edge of the rigid circular plate in the multilayered elastic solids. A local plane polar coordinate system (R,ϑ) was selected and its origin is exactly at a point $(s=1,\zeta=0,\theta=0^\circ)$ along the circular edge of the rigid plate. The relationships between the global cylindrical coordinates (r,z) and the local plane polar coordinates are defined as $s=r/a=1+R\sin\vartheta$ and $\zeta=z/a=R\cos\vartheta$, where $R\geqslant 0$ and $-90^\circ\leqslant\vartheta\leqslant 90^\circ$. One can show that if $R\approx 0$ and $R<h_1/a$, the following closed-form asymptotic results are valid for the multilayered elastic solids indented eccentrically by a rigid circular plate.

$$\mathbf{T}_z(s,\theta,\zeta)=\frac{-P_z}{2\pi a^2}\left[\phi(1)+\frac{d}{a}\psi(1)\Pi_a(\theta)\right]\begin{pmatrix}S_3\\0\\S_1+S_2\end{pmatrix}\frac{1}{\sqrt{R}}+0(\sqrt{R})$$

$$\mathbf{T}_p(s,\theta,\zeta)=\frac{-P_z}{2\pi a^2}\left[\phi(1)+\frac{d}{a}\psi(1)\Pi_a(\theta)\right]\begin{pmatrix}S_1-S_2\\0\\2\nu_1S_1\end{pmatrix}\frac{1}{\sqrt{R}}+0(\sqrt{R})$$

$$\Gamma_p(s,\theta,\zeta)=\frac{-P_z}{4\pi a^2\mu_1}\left[\phi(1)+\frac{d}{a}\psi(1)\Pi_a(\theta)\right]\begin{pmatrix}(1-2\nu_1)S_1-S_2\\0\\0\end{pmatrix}\frac{1}{\sqrt{R}}+0(\sqrt{R}) \tag{36}$$

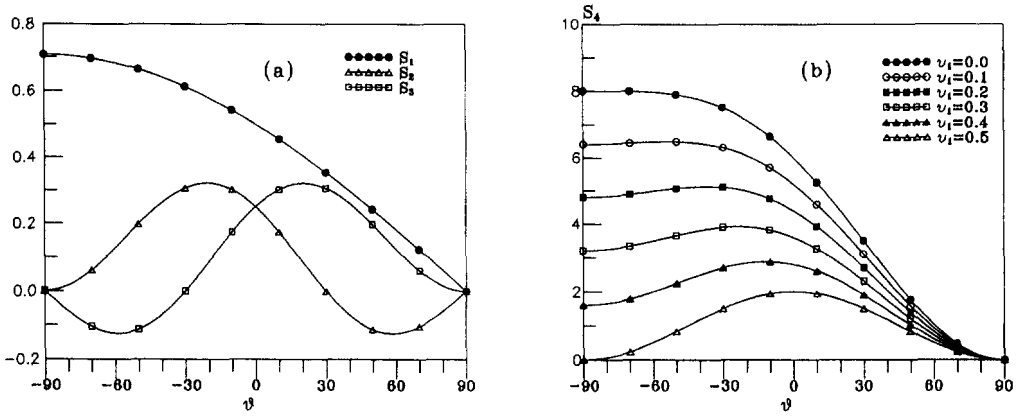

Fig. 2. Variations of the coefficient functions S_1, S_2, S_3 and S_4 vs the local tangential coordinate ϑ.

where

$$S_1 = \tfrac{1}{2}\sqrt{1-\sin\vartheta}$$
$$S_2 = \tfrac{1}{4}(\cos\vartheta - \sin 2\vartheta)\sqrt{1+\sin\vartheta}$$
$$S_3 = \tfrac{1}{4}(\cos\vartheta + \sin 2\vartheta)\sqrt{1-\sin\vartheta}. \tag{37}$$

Figure 2a illustrates the variations of S_1, S_2 and S_3 vs the local tangential coordinate ϑ. The following observations can be made from eqns (36) and (37).

1. The stresses σ_{rr}, $\sigma_{\theta\theta}$, σ_{zz}, and σ_{rz} have the singularity of $R^{-1/2}$ at the edge of the rigid plate while $\sigma_{\theta z}$, $\sigma_{\theta r}$ and $\varepsilon_{\theta\theta}$ have no singularity. At the surface $\zeta = 0$, σ_{rz} is zero.
2. The variations of the coefficients of the stress singularity vs the local coordinate ϑ are exactly the same for both the axisymmetric indentation and the central rotation of the rigid plate.
3. The effect of layering material non-homogeneity on the singular stress field near the edge of a rigid circular plate is governed by $\phi(1)$ and $\psi(1)$ for the axisymmetric indentation and central rotation of the rigid plate, respectively.
4. The variations of the coefficients of the stress singularity vs the local coordinate ϑ are independent of the material properties of the multilayered elastic solids. The variation of the coefficient of the strain singularity ($\lim_{R\to 0}\sqrt{R}\,\varepsilon_{rr}$) vs the local coordinate ϑ is dependent on the Poisson's ratio ν_1 of the first layer.

Referring to Sih (1991), a strain energy density factor S is introduced to further illustrate the effect of layering material non-homogeneity on the singular stress field at the edge of the rigid plate. The strain energy density factor S is defined as follows in the local plane polar coordinates.

$$S = \lim_{R\to 0}\frac{aR}{4\mu}\left[\sigma_{rr}^2+\sigma_{\theta\theta}^2+\sigma_{zz}^2-\frac{\nu}{1+\nu}(\sigma_{rr}+\sigma_{\theta\theta}+\sigma_{zz})^2+2(\sigma_{r\theta}^2+\sigma_{rz}^2+\sigma_{\theta z}^2)\right]. \tag{38}$$

Using eqns (36)–(38), one can express the strain energy density factors S_z and S_y, respectively, due to the axisymmetric indentation and central rotation modes, as follows.

$$S_z = \frac{P_z^2\phi^2(1)}{128\pi^2a^3\mu}S_4, \quad S_y = \frac{a^2P_z^2\psi^2(1)}{128\pi^2a^5\mu}S_4\sin^2\theta \tag{39}$$

where

$$S_4 = 5-8\nu_1-4(1-2\nu_1)\sin\vartheta+\cos 2\vartheta. \tag{40}$$

Figure 2b illustrates the variation of the function S_4 vs ϑ ($-90^\circ \leqslant \vartheta \leqslant 90^\circ$) for different values of the Poisson's ratio ν_1.

During the eccentric indentation of a rigid plate, a multilayered elastic solid may start cracking due to the stress concentration at the edge of the rigid plate. According to Sih (1991), crack initiation will start in a radial direction along which the strain energy density factor S is a maximum. Consequently, the results presented in eqns (39) and (40) indicate that cracks may initiate in the multilayered elastic solid at the edge of the rigid plate along the local radial direction of either $\vartheta = -\sin^{-1}(1-2\nu_1)$ for $0 \leqslant \nu_1 \leqslant 1/2$ or $\vartheta = -90^\circ$ for $-1 < \nu_1 \leqslant 0$. This initiation direction is because (1) for $0 \leqslant \nu_1 \leqslant 0.5$ and $\vartheta = -\sin^{-1}(1-2\nu_1)$, then $dS_4/d\vartheta = 0$ and $d^2S_4/d\vartheta^2 = -16\nu_1(1-\nu_1) \leqslant 0$ and (2) for $-1 < \nu_1 < 0$ and $\vartheta = -\pi/2$, then $dS_4/d\vartheta = 0$ and $d^2S_4/d\vartheta^2 = 8\nu_1 \leqslant 0$. These results indicate that the direction of a crack initiation at the rigid plate edge is governed only by the Poisson's ratio ν_1. The layering material non-homogeneity and the loading modes (P_z, M_y) only have the influences on the magnitude of the strain energy density factor.

8. CLOSED-FORM SOLUTION FOR AN ELASTIC HALFSPACE

It is instructive to examine the solution for a homogeneous elastic halfspace eccentrically indented by a rigid circular plate. It can be shown that the systems of Fredholm integral equations of the second kind (27) have the closed-form solutions for a homogeneous elastic halfspace, i.e., $\phi(s) = 1$ and $\psi(s) = 3s$. As a result, the elastic field in eqns (30) can be reduced to the following in the forms of elementary functions.

$$\begin{aligned}
\mathbf{u}(s,\theta,\zeta) &= \frac{-P_z}{4\pi a\mu_1}\left[\mathbf{H}_{uz}(s,\zeta)+\frac{3d}{2a}\Pi_a(\theta)\mathbf{H}_{uy}(s,\zeta)\right]\\
\mathbf{T}_z(s,\theta,\zeta) &= \frac{-P_z}{2\pi a^2}\left[\mathbf{H}_{zz}(s,\zeta)+\frac{3d}{2a}\Pi_a(\theta)\mathbf{H}_{zy}(s,\zeta)\right]\\
\Gamma_p(s,\theta,\zeta) &= \frac{-P_z}{4\pi a^2\mu_1}\left[\mathbf{H}_{pz}(s,\zeta)+\frac{3d}{2a}\Pi_a(\theta)\mathbf{H}_{py}(s,\zeta)\right]
\end{aligned} \tag{41}$$

where $0 \leqslant \zeta, s < \infty$, $0 \leqslant \theta < 2\pi$. The kernel matrix functions $\mathbf{H}_{uz}$, $\mathbf{H}_{uy}$, $\mathbf{H}_{zz}$, $\mathbf{H}_{zy}$, $\mathbf{H}_{pz}$, and $\mathbf{H}_{py}$ are given by

$$\mathbf{H}_{uz} = \begin{pmatrix} (1-2\nu_1)Z_{10}-\zeta Z_{11} \\ 0 \\ 2(\nu_1-1)Z_{00}-\zeta Z_{01} \end{pmatrix}, \quad \mathbf{H}_{uy} = \begin{pmatrix} (2\nu_1-1)(Y_{00}-Y_{20})+\zeta(Y_{01}-Y_{21}) \\ (1-2\nu_1)(Y_{00}+Y_{20})-\zeta(Y_{01}+Y_{21}) \\ 4(\nu_1-1)Y_{10}-2\zeta Y_{11} \end{pmatrix}$$

$$\mathbf{H}_{zz} = \begin{pmatrix} \zeta Z_{12} \\ 0 \\ Z_{01}+\zeta Z_{02} \end{pmatrix}, \quad \mathbf{H}_{pz} = \frac{1}{2}\begin{pmatrix} (2\nu_1-1)(Z_{21}-Z_{01})+\zeta(Z_{22}-Z_{02}) \\ 0 \\ (1-2\nu_1)(Z_{21}+Z_{01})-\zeta(Z_{22}+Z_{02}) \end{pmatrix}$$

$$\mathbf{H}_{zy} = \begin{pmatrix} -\zeta(Y_{02}-Y_{22}) \\ \zeta(Y_{02}+Y_{22}) \\ 2(Y_{11}+\zeta Y_{12}) \end{pmatrix}, \quad \mathbf{H}_{py} = \frac{1}{2}\begin{pmatrix} (2\nu_1-1)(Y_{31}-3Y_{11})+\zeta(Y_{32}-3Y_{12}) \\ (2\nu_1-1)(Y_{31}+Y_{11})+\zeta(Y_{32}+Y_{12}) \\ (1-2\nu_1)(Y_{31}+Y_{11})-\zeta(Y_{32}+Y_{12}) \end{pmatrix} \tag{42}$$

where Z_{mk} and Y_{mk} ($m = 0, 1, 2, 3$; $k = 0, 1, 2$) are non-dimensionally elementary functions of s and ζ and are given in the Appendix A. It can be shown that these results in equations

(42) and (43) are identical to those obtained from classical elastostatics (see, e.g., Boussinesq, 1885; Sneddon and Harding, 1945; Sneddon, 1946; Gladwell, 1980).

9. NUMERICAL EVALUATION

Considering the structure of the kernel functions (28), it is unlikely that the systems of Fredholm integral equations of the second kind (27) will have exact solutions. In this paper, the following numerical scheme was adopted for the evaluation of the solutions of the Fredholm integral equations of the second kind (Yue, 1992; Yue and Selvadurai, 1994). The interval [0, 1] is divided into N segments with ends defined by $s_k = (k-1)/N$; $k = 1, 2, 3, \ldots, (N+1)$, and the collocation points are $x_k = (s_k + s_{k+1})/2$, $k = 1, 2, 3, \ldots, N$. Consequently we can convert the integral equations into two systems of linear algebraic equations. These linear algebraic equations can be written in the following generalized matrix form.

$$\sum_{k=1}^{N+1} [\mathbf{A}_{lk}][\mathbf{X}_k] = [\mathbf{B}_l] \tag{43}$$

where $l = 1, 2, 3, \ldots, N, N+1$. The eqns (44) are solved numerically to generate the unknown variables $\phi(x_k)$ $(k = 1, 2, 3, \ldots, N)$ and X_z for the axial translation and $\psi(x_k)$ $(k = 1, 2, 3, \ldots, N)$ and X_γ for the central rotation of the rigid plate. The solution of the elastic field induced by the eccentric indentation of the rigid plate can be further evaluated using eqns (30)–(36) and the numerical results of eqns (44).

The numerical techniques adopted here involve three computational steps. The first step is the evaluation of the solution in the transform domain (15)–(18). It is noted that $\Phi(\rho, z)$ and $\Psi(\rho, z)$ in eqns (15) have no functions of exponential growth. This property ensures that the calculation of the kernel functions is stable and can be very accurate for any arbitrary combination of dissimilar elastic layers in the multilayered solid (Yue, 1995).

The second step involves the numerical integration of the semi-infinite integrals in eqns (28) and (32). The semi-infinite limit of the integrals was handled using a proceeding limit technique. Furthermore, as the evaluation depth becomes near the surface (ζ is small), the integrands in eqns (32) will very slowly converge to zero as ρ becomes large. This property of the integrands will slow the convergence of the numerical integration and render the numerical integration procedure unstable. This numerical problem is overcome by using an asymptotic technique which separates the integrands into two parts. The first part relates to the asymptotic functions as ρ is very large. The second relates to the difference between the integrands and their asymptotic functions. Closed-form results can be obtained for the infinite integrals associated with asymptotic functions. The proceeding limit technique, which is based on an adaptively iterative Simpson's quadrature, was used for the evaluation of the infinite integrals associated with the remaining terms. The details of these two techniques are documented in the Appendix B.

The third numerical step involves the systems of Fredholm integral equations of the second kind (27) and the solution of the elastic field (30) and (33). The numerical solutions of the integral eqns (44) have been well investigated by many researchers (see, for examples, Baker, 1977; Delves and Mohamed, 1985). These studies show that with the increase in the segment number N it is possible to obtain more accurate and readily convergent solutions for the integral equations.

Based on the above discussions, the following equations were applied to numerical evaluation of the elastic field. (i) For $\zeta \geqslant H_1$, a and $s \geqslant 0$, the following numerical integration was used.

$$\int_0^1 \phi(t)\mathbf{K}_{bz}(s, \zeta, t)\,\mathrm{d}t \approx \sum_{k=1}^{N} \phi(t_k)\mathbf{K}_{bz}(s, \zeta, t_k)/N$$

$$\int_0^1 \psi(t)\mathbf{K}_{b\gamma}(s, \zeta, t)\,\mathrm{d}t \approx \sum_{k=1}^{N} \psi(t_k)\mathbf{K}_{b\gamma}(s, \zeta, t_k)/N \tag{44}$$

where $\mathbf{K}_{bz} = \mathbf{K}_{uz}, \mathbf{K}_{zz}, \mathbf{K}_{pz}$; and $\mathbf{K}_{by} = \mathbf{k}_{ur}, \mathbf{K}_{zy}, \mathbf{K}_{py}$. (ii) For $0 < \zeta < H_1/a$ and $s \geqslant 0$, the following equations were used to more accurately calculate the results.

$$\int_0^1 \phi(t)\mathbf{K}_{bz}(s,\zeta,t)\,\mathrm{d}t \approx \sum_{k=1}^{N} \phi(t_k)\mathbf{K}^d_{bz}(s,\zeta,t_k)/N + \int_0^1 \phi(t)\mathbf{K}^a_{bz}(s,\zeta,t)\,\mathrm{d}t$$

$$\int_0^1 \psi(t)\mathbf{K}_{by}(s,\zeta,t)\,\mathrm{d}t \approx \sum_{k=1}^{N} \psi(t_k)\mathbf{K}^d_{by}(s,\zeta,t_k)/N + \int_0^1 \psi(t)\mathbf{K}^a_{by}(s,\zeta,t)\,\mathrm{d}t \tag{45}$$

where $\mathbf{K}^a_{bz}$ and $\mathbf{K}^a_{by}$ are the closed-form results associated with asymptotic functions; and $\mathbf{K}^d_{bz}$ and $\mathbf{K}^d_{by}$ are the kernel functions associated with the remaining terms (see Appendices A and B). The integrals in eqns (46) associated with the asymptotic functions can be accurately calculated using the Simpson's quadrature based adaptively iterative integration. (iii) For $\zeta = 0$, the eqns (46) were used again. However, special treatment was given to the weak singularity of the integrands associated with the functions $F_2(s,t)$ and $F_3(s,t)$ in eqns (35). In particular, the following equations were used for the evaluation of the singular functions $G_1(s)$ and $G_2(s)$ $(0 < s < 1)$.

$$G_1(s) = \frac{\phi(1)}{\sqrt{1-s^2}} - \int_s^1 \left[\frac{\mathrm{d}\phi(t)}{\mathrm{d}t} - \frac{\mathrm{d}\phi(s)}{\mathrm{d}s}\right]\frac{\mathrm{d}t}{\sqrt{t^2-s^2}} - \frac{\mathrm{d}\phi(s)}{\mathrm{d}s}[\ln(1+\sqrt{1-s^2}) - \ln(s)]$$

$$G_2(s) = \frac{s\psi(1)}{\sqrt{1-s^2}} - s\int_s^1 \left[\frac{\mathrm{d}}{\mathrm{d}t}\left(\frac{\psi(t)}{t}\right) - \frac{\mathrm{d}}{\mathrm{d}s}\left(\frac{\psi(s)}{s}\right)\right]\frac{\mathrm{d}t}{\sqrt{t^2-s^2}} - s\frac{\mathrm{d}}{\mathrm{d}s}\left(\frac{\psi(s)}{s}\right)[\ln(1+\sqrt{1-s^2}) - \ln(s)]. \tag{46}$$

The definite integrals in the above equations are proper and can be easily calculated.

In the above evaluation, the functions $\phi(s)$ and $\psi(s)$ and their derivatives $\mathrm{d}\phi(s)/\mathrm{d}s$ and $\mathrm{d}/\mathrm{d}s(\psi(s)/s)$ were calculated from their values at the collocation points x_k $(k = 1, 2, 3, \ldots, N)$ using the three points Lagrange's interpolation.

10. VERIFICATION OF NUMERICAL SOLUTIONS

Due to the accumulations of the errors in each repeated numerical integration, numerical results are presented in the ensuing to verify the techniques adopted in this study. It is noted that the contact problem of the eccentrically loaded rigid plate on a multilayered elastic solid decouples into two symmetrical problems of an axisymmetric indentation mode P_z and a central rotation mode M_y. As a result, the numerical results can be more clearly presented in terms of the two deformation modes of axisymmetric indentation and central rotation of the rigid plate. Furthermore, the tangential variation of the elastic field associated with the central rotation mode is governed by the matrix $\Pi_a(\theta)$ in eqns (31). Because the elements of $\Pi_a(\theta)$ are the elementary functions of sine and cosine, the presentation of the numerical results will focus on the variation of the solution with the radial and vertical coordinates $s(= r/a)$ and $\zeta(= z/a)$.

10.1. *Convergence of the numerical solutions*

A model of a six-layered elastic pavement was employed as an example. Referring to Bush and Baladi (1989), the properties of the six elastic pavement layers were selected as follows: $\{h_j/a\} = \{0.3, 0.7, 1.0, 1.0, 1.3, \infty\}$; $\{\mu_j/\mu\} = \{1, 0.5, 0.2, 0.09, 0.05, 0.01\}$; and $\{v_j\} = \{0.35, 0.3, 0.25, 0.4, 0.45, 0.5\}$, where $j = 1$–6. The convergence of the numerical solu-

Table 1. Effect of N on the convergence of the numerical solution of $\phi(s)$ and $\psi(s)$

s	$N = 5$ $\phi(s)$	$N = 15$ $\phi(s)$	$N = 30$ $\phi(s)$	$N = 50$ $\phi(s)$	$N = 100$ $\phi(s)$
0.0	0.76728	0.75924	0.75890	0.75883	0.75881
0.1	0.76709	0.76370	0.76340	0.76333	0.76330
0.2	0.77960	0.77744	0.77716	0.77710	0.77707
0.3	0.80482	0.80144	0.80113	0.80107	0.80105
0.4	0.83686	0.83760	0.83741	0.83736	0.83734
0.5	0.89339	0.89037	0.89008	0.89004	0.89002
0.6	0.96313	0.96636	0.96639	0.99632	0.96629
0.7	1.07994	1.07724	1.07702	1.07693	1.07692
0.8	1.24382	1.23480	1.23438	1.23429	1.23426
0.9	1.45477	1.44650	1.44573	1.44559	1.44553
1.0	1.71280	1.70737	1.70447	1.70396	1.70379
s	$\psi(s)$	$\psi(s)$	$\psi(s)$	$\psi(s)$	$\psi(s)$
0.0	0.01836	0.00040	0.00005	0.00001	0.00000
0.1	0.21917	0.21531	0.21495	0.21488	0.21485
0.2	0.43817	0.43470	0.43411	0.43398	0.43392
0.3	0.67533	0.66375	0.66268	0.66248	0.66239
0.4	0.91384	0.90938	0.90826	0.09800	0.90788
0.5	1.20418	1.18486	1.18306	1.18273	1.18259
0.6	1.51583	1.50819	1.50675	1.50623	1.50602
0.7	1.94034	1.91013	1.90746	1.90678	1.90655
0.8	2.47771	2.42203	2.41832	2.41748	2.41714
0.9	3.12795	3.06722	3.06168	3.06056	3.06008
1.0	3.89105	3.83949	3.82855	3.82642	3.82560

Table 2. Effect of N on the convergence of the derivatives of $\phi(s)$ and $\psi(s)$

s	$N = 5$ $d\phi(s)/ds$	$N = 15$ $d\phi(s)/ds$	$N = 30$ $d\phi(s)/ds$	$N = 50$ $d\phi(s)/ds$	$N = 100$ $d\phi(s)/ds$
0.0	−0.06554	−0.00156	−0.00019	−0.00004	−0.00001
0.1	0.06156	0.09081	0.09042	0.09041	0.09040
0.2	0.18866	0.18665	0.18647	0.18643	0.18641
0.3	0.31576	0.29857	0.29666	0.29658	0.29655
0.4	0.44286	0.43662	0.43605	0.43593	0.43588
0.5	0.68781	0.63604	0.63005	0.62984	0.62976
0.6	0.93275	0.91587	0.91433	0.91400	0.91387
0.7	1.40346	1.33007	1.32117	1.32070	1.32050
0.8	1.87417	1.84374	1.84103	1.84045	1.84021
0.9	2.34487	2.36839	2.37491	2.37437	2.37415
1.0	2.81558	2.84890	2.78017	2.76157	2.75315
s	$\frac{d[\psi(s)/s]}{ds}$	$\frac{d[\psi(s)/s]}{ds}$	$\frac{d[\psi(s)/s]}{ds}$	$\frac{d[\psi(s)/s]}{ds}$	$\frac{d[\psi(s)/s]}{ds}$
0.0	−0.19272	−0.00524	−0.00063	−0.00014	−0.00002
0.1	0.05204	0.13708	0.13582	0.13577	0.13575
0.2	0.29680	0.29070	0.29014	0.29002	0.28997
0.3	0.54156	0.49311	0.48769	0.48748	0.48739
0.4	0.78631	0.76682	0.76503	0.76466	0.76450
0.5	1.30205	1.18541	1.17217	1.17154	1.17127
0.6	1.81778	1.76566	1.76095	1.75995	1.75923
0.7	2.66785	2.55565	2.54318	2.54173	2.54112
0.8	3.51792	3.42262	3.41413	3.41233	3.41157
0.9	4.36799	4.08638	4.10608	4.10424	4.10347
1.0	5.21806	4.56970	4.37676	4.33185	4.31273

tion was verified by considering the influence of the segment number N in eqns (44) and the relative/or absolute error ε_a (eqn (B2)) of the numerical integration. Some of the results are presented in Tables 1–4, where N was 5, 15, 30, 50, or 100 and ε_a was 10^{-4} in the calculation. Furthermore, the patterns of the above numerical results are illustrated in Fig. 3,

Table 3. Effect of N on the convergence of the vertical surface deflection

s	$N = 5$ $a\mu u_z(s)/P_z$	$N = 15$ $a\mu u_z(s)/P_z$	$N = 30$ $a\mu u_z(s)/P_z$	$N = 50$ $a\mu u_z(s)/P_z$	$N = 100$ $a\mu u_z(s)/P_z$
0.0	2.24438	2.24206	2.24184	2.24180	2.24178
1.0	2.24438	2.24206	2.24184	2.24180	2.24178
1.01	2.21896	2.21695	2.21674	2.21670	2.21669
1.05	2.18616	2.18441	2.18424	2.18420	2.18419
1.1	2.15939	2.15791	2.15777	2.15774	2.15773
1.15	2.13715	2.13589	2.13577	2.13574	2.13573
1.2	2.11713	2.11606	2.11596	2.11593	2.11592
1.25	2.09856	2.09763	2.09754	2.09752	2.09752
1.3	2.08107	2.08025	2.08017	2.08016	2.08015
1.4	2.04861	2.04794	2.04788	2.04786	2.04786
1.5	2.01883	2.01823	2.01818	2.01817	2.01816
2.0	1.89427	1.89385	1.89381	1.89380	1.89380
2.5	1.79167	1.79134	1.79131	1.79131	1.79130
3.0	1.70121	1.70096	1.70094	1.70093	1.70093
4.0	1.54342	1.54325	1.54323	1.54323	1.54323
5.0	1.40651	1.40637	1.40636	1.40636	1.40636
s	$a^2\mu u_z(s)/M_y$	$a^2\mu u_z(s)/M_y$	$a^2\mu u_z(s)/M_y$	$a^2\mu u_z(s)/M_y$	$a^2\mu u_z(s)/M_y$
0.0	0.00000	0.00000	0.00000	0.00000	0.00000
1.0	0.53825	0.53048	0.52977	0.52962	0.52956
1.01	0.48544	0.47931	0.47869	0.47856	0.47851
1.05	0.43221	0.42726	0.42677	0.42667	0.42663
1.1	0.39787	0.39389	0.39350	0.39342	0.39338
1.15	0.37357	0.37033	0.37002	0.36995	0.36993
1.2	0.35407	0.35142	0.35117	0.35111	0.35109
1.25	0.33756	0.33537	0.33515	0.33511	0.33509
1.3	0.32320	0.32136	0.32118	0.32114	0.32113
1.4	0.29930	0.29791	0.29778	0.29775	0.29774
1.5	0.28019	0.27907	0.27896	0.27894	0.27893
2.0	0.22300	0.22240	0.22234	0.22233	0.22232
2.5	0.19274	0.19236	0.19233	0.19232	0.19232
3.0	0.17276	0.17250	0.17248	0.17248	0.17247
4.0	0.14675	0.14661	0.14659	0.14659	0.14659
5.0	0.12920	0.12911	0.12908	0.12908	0.12908

where N used was 100. In Table 3 and Fig. 3(b), $a\mu u_z(s)/P_z$ and $a^2\mu u_z(s)/M_y$ indicate the non-dimensional vertical surface deflections associated with the axisymmetric indentation mode and the central rotation mode, respectively. Similarly, in Table 4 and Fig. 3(c), $a^2\sigma_{zz}(s)/P_z$ and $a^3\sigma_{zz}(s)/M_y$ indicate the non-dimensional contact normal stress associated with the axisymmetric indentation mode and the central rotation mode, respectively.

The results listed in these tables indicate that the numerical solutions of $\phi(s)$ and $\psi(s)$, the derivatives $\mathrm{d}\phi(s)/\mathrm{d}s$ and $\mathrm{d}[\psi(s)/s]/\mathrm{d}s$, the vertical surface deflection and the contact normal stress converge quickly and stably as the increase of the segment number N. In particular, Fig. 3b and Fig. 3c also illustrate the vertical surface deflections and the normal contact stresses associated with a six-layered elastic pavement model where the sixth elastic layer is not of semi-infinite extent, but, has a limit thickness of $h_6/a = 20.0$, and either smoothly or roughly rests on a rigid base. The results indicate that the base condition has an effect on the vertical surface deflection associated with the axisymmetric indentation mode, but a very limited effect on the surface deflection associated with the central rotation mode and on the contact normal stress associated with the both basic modes.

10.2. *Accuracy of the numerical solutions*

The results given by Gao *et al.* (1992) for the contact compliance of a one or two layered elastic halfspace were used as the first example for the verification of the accuracy

Table 4. Effect of N on the convergence of the normal contact stress

s	$N = 5$ $-a^2\sigma_{zz}(s)$ / $10^{-2}P_z$	$N = 15$ $-a^2\sigma_{zz}(s)$ / $10^{-2}P_z$	$N = 30$ $-a^2\sigma_{zz}(s)$ / $10^{-2}P_z$	$N = 50$ $-a^2\sigma_{zz}(s)$ / $10^{-2}P_z$	$N = 100$ $-a^2\sigma_{zz}(s)$ / $10^{-2}P_z$
0.0	−0.70971	2.52499	2.66226	2.68281	2.68958
0.01	4.82055	2.65548	2.67687	2.68518	2.68898
0.1	2.58602	2.70414	2.76299	2.77370	2.77780
0.2	2.37146	2.97328	3.03295	3.04397	3.04835
0.3	2.79434	3.44316	3.50840	3.52000	3.52448
0.4	3.56872	4.19759	4.26157	4.27354	4.27818
0.5	4.74367	5.42035	5.49051	5.50198	5.50642
0.6	7.21502	7.64044	7.69163	7.70075	7.70417
0.7	11.63178	11.98220	12.02165	12.02555	12.02669
0.8	21.35027	21.17469	21.17261	21.16918	21.16702
0.85	29.91503	29.55578	29.54635	29.53924	29.53530
0.9	43.94660	43.54968	43.52943	43.52072	43.51577
0.95	73.63420	73.20316	73.23769	73.22789	73.22137
0.97	101.38839	100.90923	100.91208	100.91202	100.90536
0.99	186.94853	186.26203	186.07539	186.05256	186.04552
s	$-a^3\sigma_{zz}(s)$ / $10^{-2}M_z$	$-a^3\sigma_{zz}(s)$ / $10^{-2}M_z$	$-a^3\sigma_{zz}(s)$ / $10^{-2}M_z$	$-a^3\sigma_{zz}(s)$ / $10^{-2}M_z$	$-a^3\sigma_{zz}(s)$ / $10^{-2}M_z$
0.0	0.00000	0.00000	0.00000	0.00000	0.00000
0.01	0.24178	0.18054	0.18013	0.18013	0.18015
0.1	1.74804	1.80353	1.81176	1.81265	1.81289
0.2	3.29105	3.68013	3.69620	3.69800	3.69853
0.3	5.11401	5.73144	5.75829	5.76099	5.76173
0.4	7.39879	8.17614	8.20663	8.20977	8.21055
0.5	10.46147	11.48545	11.52434	11.52634	11.52647
0.6	15.94308	16.83680	16.85118	16.84851	16.84647
0.7	25.82125	26.81193	26.79694	26.78399	26.77725
0.8	46.60055	47.50156	47.42262	47.39399	47.37996
0.85	65.35445	66.32565	66.22702	66.18702	66.16763
0.9	96.75497	97.75708	97.61536	97.56857	97.54530
0.95	164.31193	164.38384	164.34465	164.28052	164.24707
0.97	227.76338	226.69090	226.52268	226.46636	226.42594
0.99	423.05637	418.69337	417.86184	417.70668	417.64428

of the numerical solutions obtained in this study. Tables 5 and 6 illustrate the comparison of results for the contact compliance $4a\mu_2 D_z/(1-\nu_1)P_z$. The digital results of Gao *et al.* (1992) in Tables 5 and 6 were estimated from Fig. 2 in the paper of Gao *et al.* (1992). As is evident, the results of the current study are well consistent with the results obtained by Gao *et al.* (1992) from a finite element analysis. Figure 4 also illustrates the contact compliance of a one or two layered elastic halfspace for a wide range of the shear modulus ratio μ_1/μ_2 of a one-layered elastic halfspace or the shear modulus ratio μ_1/μ_3 of a two-layered elastic halfspace.

The second example is to verify the contact normal stress beneath a rigid plate, where the results given by Chen and Engel (1972) are used for comparison. Figure 5a illustrates the non-dimensional pressure distribution under a rigid circular plate for the axisymmetrical indentation of the rigid plate at the surface of a one-layered elastic halfspace. In Fig. 5(a), the ratio of h_1/a is 0.2, 0.3, 0.4, 0.5, 1, 1.5, 2, or ∞. It is evident that the results in Fig. 5(a), for the cases of $h_1/a = 0.3$, 0.5, 1, 2, or ∞, are exactly the same as those in Fig. 6 of Chen and Engel (1972) using a least-squares approach. As observed by Chen and Engel (1972), when the first layer becomes thinner, i.e., $h_1/a = 1$, 0.5, there is a central region where the normal stress between the layer and the plate is tensile. When the layer is still thinner, i.e., $h_1/a = 0.4$, 0.3, 0.2, this region of tensile contact stress becomes an annular strip. Figure 5(b) illustrates the non-dimensional pressure distribution under a rigid circular plate for

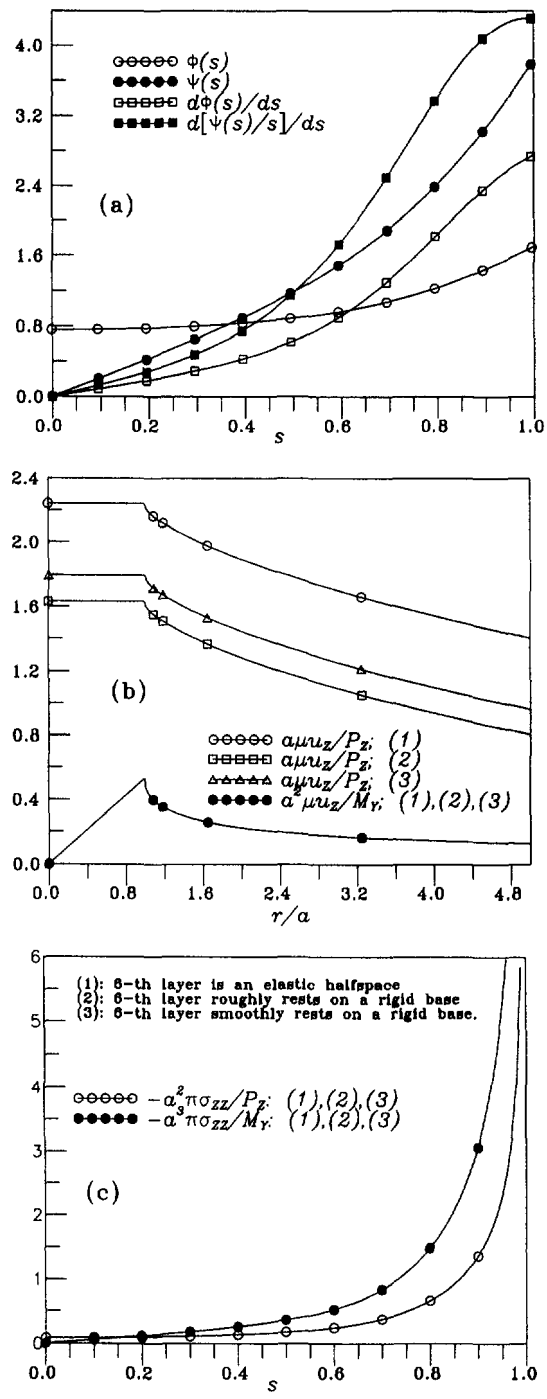

Fig. 3. Solution of the integral equation, surface deflection and normal contact stress for a five-layered elastic halfspace.

the central rotation of the rigid plate at the surface of a one-layered elastic halfspace, where $\theta = 0$.

In the calculation of the above two examples, the segment number N was 100 and the error of numerical integration ε_a was 10^{-4}. From the results presented above, it can be concluded that the numerical scheme and techniques adopted in this study provide highly stable and accurate solutions for the mix boundary value problem of classical elasticity in multilayered solids.

Table 5. A comparison between the results of axial indentation $4a\mu_2 D_z/(1-\nu_1)/P_z$ given by (1) the current study and (2) Gao *et al.* (1992) for one-layered halfspace

h_1/a	0.5	0.5	1.0	1.0	3.0	3.0	7.0	7.0
μ_1/μ_2	(1)	(2)	(1)	(2)	(1)	(2)	(1)	(2)
0.5	1.27469	1.272	1.44753	1.440	1.75298	1.784	1.88924	1.876
0.6	1.18632	1.180	1.30136	1.256	1.50381	1.448	1.59369	1.580
0.7	1.12168	1.112	1.19553	1.180	1.32497	1.312	1.38218	1.372
0.8	1.07202	1.060	1.11505	1.104	1.19016	1.180	1.22322	1.212
1.0	1.00000	1.000	1.00000	1.000	1.00000	1.000	1.00000	1.000
1.7	0.86947	0.860	0.79899	0.792	0.67983	0.672	0.62905	0.620
1.8	0.85797	0.848	0.78191	0.772	0.65375	0.648	0.59929	0.592
1.9	0.84745	0.836	0.76640	0.760	0.63028	0.624	0.57260	0.568
2.0	0.83777	0.828	0.75223	0.744	0.60902	0.612	0.54853	0.548

Table 6. A comparison between the results of axial indentation $4a\mu_3 D_z/(1-\nu_1)/P_z$ given by (1) the current study and (2) Gao *et al.* (1992) for two-layered halfspace

h_1/a	0.5	0.5	1.0	1.0	3.0	3.0	7.0	7.0
μ_1/μ_2	(1)	(2)	(1)	(2)	(1)	(2)	(1)	(2)
0.5	1.33414	1.330	1.51823	1.526	1.79445	1.762	1.90853	1.897
0.6	1.23047	1.223	1.35361	1.358	1.53418	1.509	1.60780	1.600
0.7	1.15259	1.142	1.23194	1.231	1.34596	1.325	1.39191	1.382
0.8	1.09134	1.081	1.13771	1.138	1.20313	1.186	1.22923	1.215
1.0	1.00000	1.000	1.00000	1.000	1.00000	1.000	1.00000	1.000
1.7	0.82617	0.823	0.74979	0.754	0.65304	0.649	0.61676	0.615
1.8	0.81038	0.800	0.72800	0.730	0.62451	0.621	0.58590	0.578
1.9	0.79590	0.790	0.70817	0.709	0.59882	0.594	0.55820	0.554
2.0	0.78254	0.778	0.69003	0.689	0.57555	0.586	0.53321	0.530

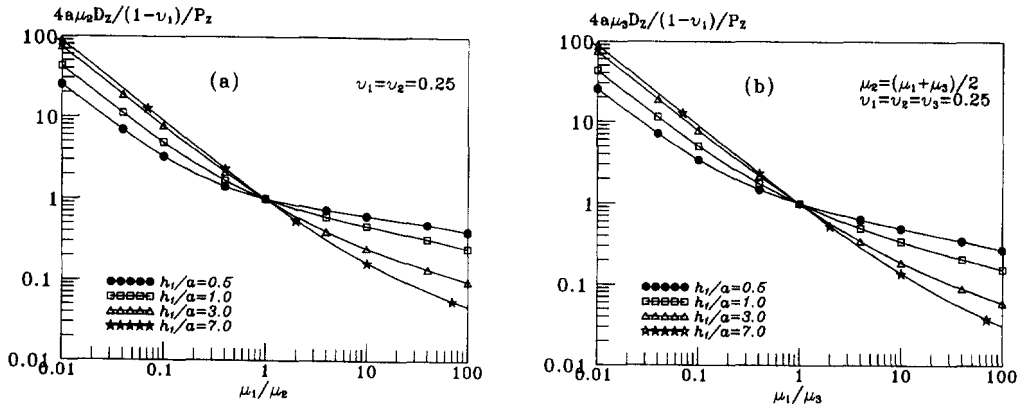

Fig. 4. Variations of a rigid plate loading compliance vs shear modulus ratio for a one-layered elastic halfspace (a) or a two-layered elastic halfspace (b).

11. FURTHER NUMERICAL RESULTS

In the ensuing further numerical results are presented to illustrate the influence of layering material inhomogeneity on the elastic field induced by the eccentric loading of a rigid plate. The pavement model of a five-layered elastic halfspace is employed again as an example (see Section 10.1). The elastic field in the five-layered elastic halfspace due to axisymmetric indentation of the rigid plate is presented in Figs 6, 8, 10, 12 and 14 while the elastic field due to the central rotation mode is presented in Figs 7, 9, 11, 13 and 15. In the calculation of the numerical results, the segment number N was 100 and the error of numerical integration ε_a was 10^{-5}. For comparison purpose, the corresponding elastic field

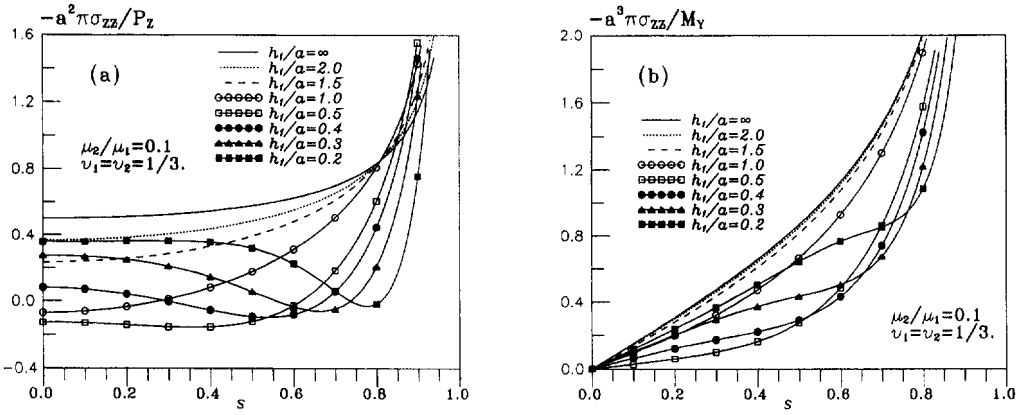

Fig. 5. Normal pressure distribution under a rigid plate punch for a one-layered elastic halfspace.

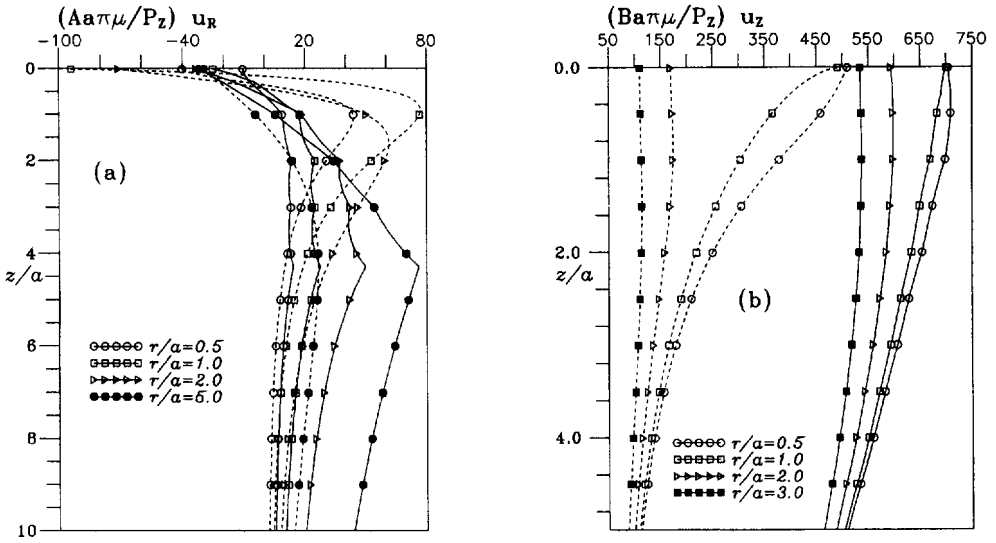

Fig. 6. Displacements vs depth for either a five-layered halfspace (solid line, $A = B = 100$) or a homogeneous halfspace (dashed line, $A = 2000$, $B = 1000$) axisymmetrically indented by a rigid plate.

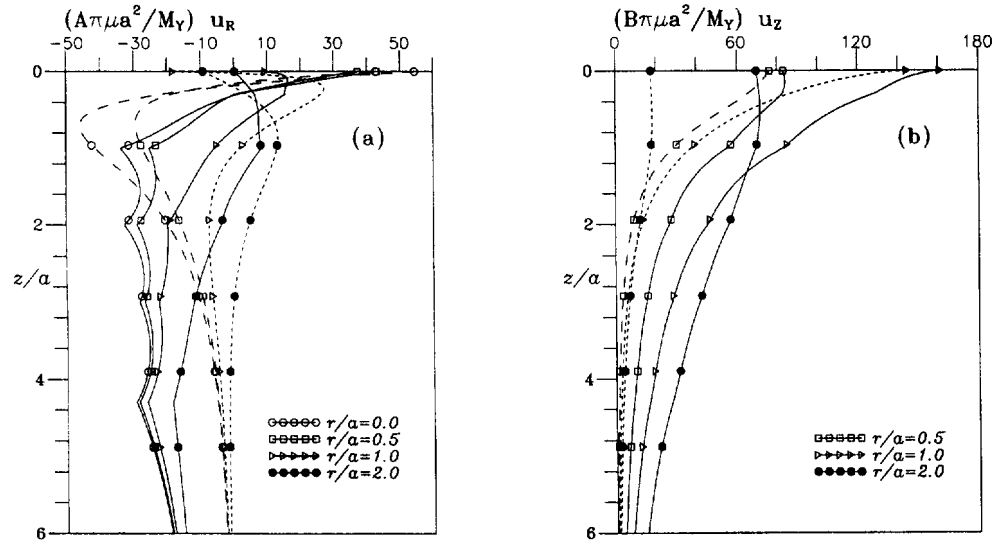

Fig. 7. Displacements vs depth for either a five-layered halfspace (solid line, $A = B = 100$) or a homogeneous halfspace (dashed line, $A = 500$, $B = 200$) rotationally indented by a rigid plate.

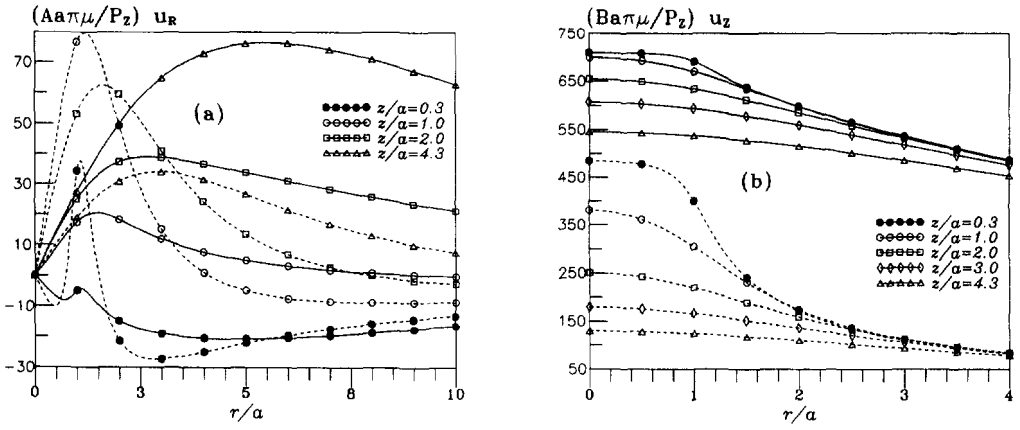

Fig. 8. Displacements vs radial distance for either a five-layered halfspace (solid line, $A = B = 100$) or a homogeneous halfspace (dashed line, $A = 2000$, $B = 1000$) axisymmetrically indented by a rigid plate.

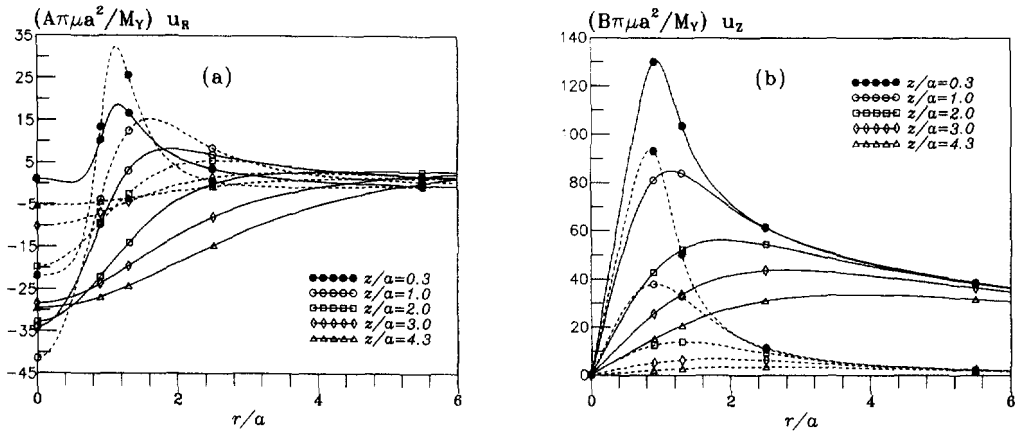

Fig. 9. Displacements vs radial distance for either a five-layered halfspace (solid line, $A = B = 100$) or a homogeneous halfspace (dashed line, $A = 500$, $B = 200$) rotationally indented by a rigid plate.

is also presented in these figures for a homogeneous elastic halfspace ($\mu_1 = \mu$, $\nu_1 = 0.35$) induced by the axisymmetric and rotational indentation of the rigid plate.

Figures 6 and 7 illustrate respectively the variations of the non-dimensional displacements ($a\pi\mu u_r/P_z$, $a\pi\mu u_z/P_z$) and ($a^2\pi\mu u_r/M_y$, $a^2\pi\mu u_z/M_y$) vs the depth z/a in both the five-layered and the homogeneous elastic halfspaces. The displacements in the homogeneous elastic halfspace are decaying much faster with the depth and have much smaller values than those in the five-layered elastic halfspace. The displacements due to the central rotation M_y are decaying much faster with the depth than those due to the axisymmetric indentation P_z. At the interfaces $z/a = 0.3$, 1.0, 2.0, 3.0, and 4.3, the gradients of the displacements are not continuous for those in the five-layered elastic halfspace and are continuous for those in the homogeneous elastic halfspace.

Figures 8 and 9 illustrate respectively the variations of the non-dimensional displacements ($a\pi\mu u_r/P_z$, $a\pi\mu u_z/P_z$) and ($a^2\pi\mu u_r/M_y$, $a^2\pi\mu u_z/M_y$) vs the radial distance r/a at the interface depths in the elastic halfspaces. The displacements in the homogeneous elastic halfspace are decaying much faster with the radial distance than those in the five-layered elastic halfspace. The displacements due to the central rotation M_y are decaying much faster with the radial distance than those due to the axisymmetric indentation P_z.

Figures 10 and 11 illustrate the variations of the non-dimensional stresses vs the depth z/a in the two elastic halfspaces induced by P_z and M_y, respectively. The vertical stresses

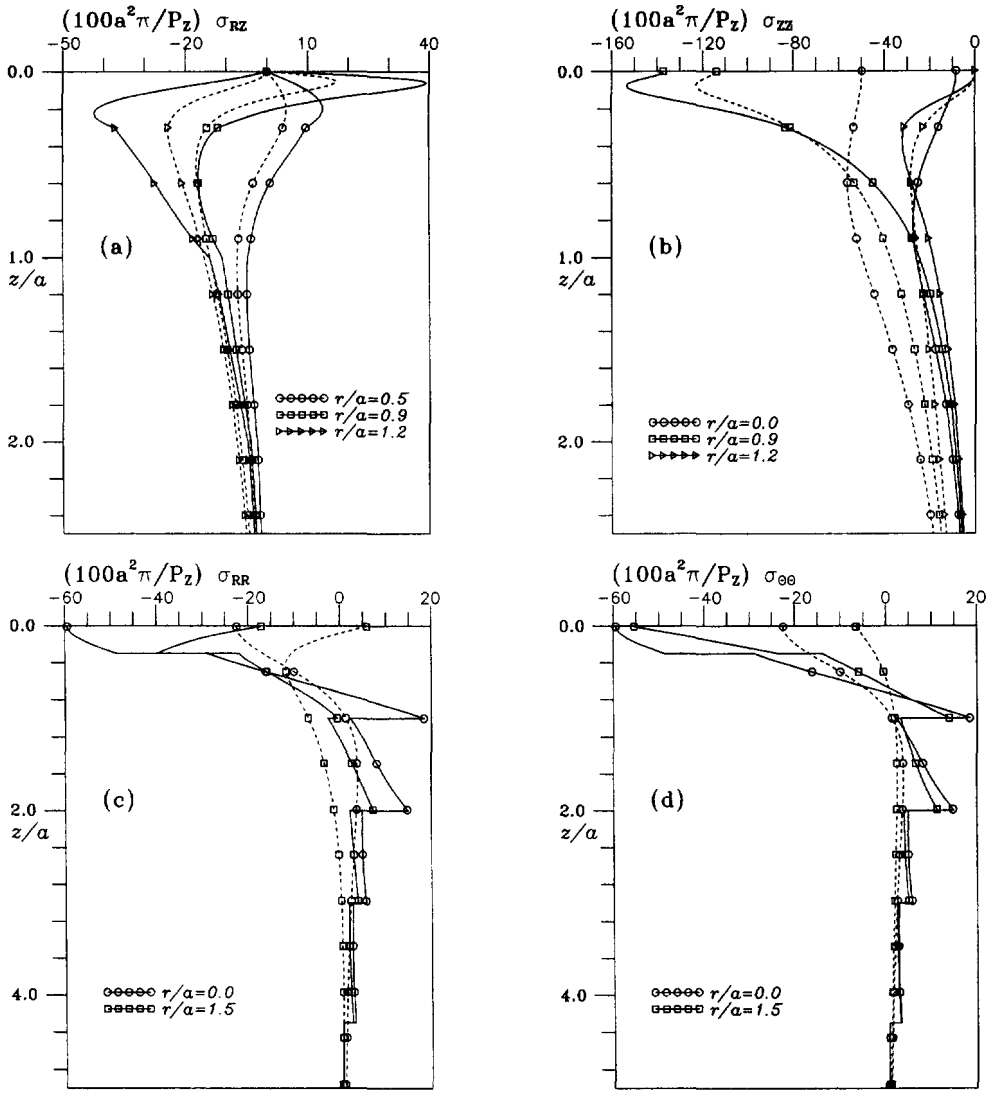

Fig. 10. Stresses vs depth for either a five-layered halfspace (solid line) or a homogeneous halfspace (dashed line) axisymmetrically indented by a rigid plate.

(σ_{rz} and σ_{zz}) in the homogeneous elastic halfspace are decaying slower with the depth than those in the five-layered elastic halfspace and have more or less the same values of the latter. At the interfaces $z/a = 0.3$, 1.0, 2.0, 3.0, and 4.3, the gradients of the vertical stresses are not continuous for those in the five-layered elastic halfspace and are continuous for those in the homogeneous elastic halfspace. The horizontal normal stresses (σ_{rr} and $\sigma_{\theta\theta}$) in the two solids have quite different patterns of the variations with the depth. The normal horizontal stresses in the five-layered elastic halfspace have the discontinuity of the first kind across the interfaces. Very high tensile stresses are generated for the horizontal normal stresses at the bottom of each layer in the five-layered elastic halfspace.

Figures 12 and 13 illustrate the variations of the non-dimensional vertical stresses (σ_{rz} and σ_{zz}) vs the radial distance r/a at the first three interfaces ($z/a = 0.3$, 1.0 and 2.0) in the two elastic halfspaces induced by P_z and M_y, respectively. The vertical stresses in the homogeneous elastic halfspace are decaying slower with the radial distance than those in the five-layered elastic halfspace and have more or less the same values of the latter.

Figures 14 and 15 present a detailed illustration of the discontinuity of the horizontal normal stresses (σ_{rr} and $\sigma_{\theta\theta}$) at the interfaces $z/a = 0.3$, 1.0, 2.0, 3.0, and 4.3 in both the

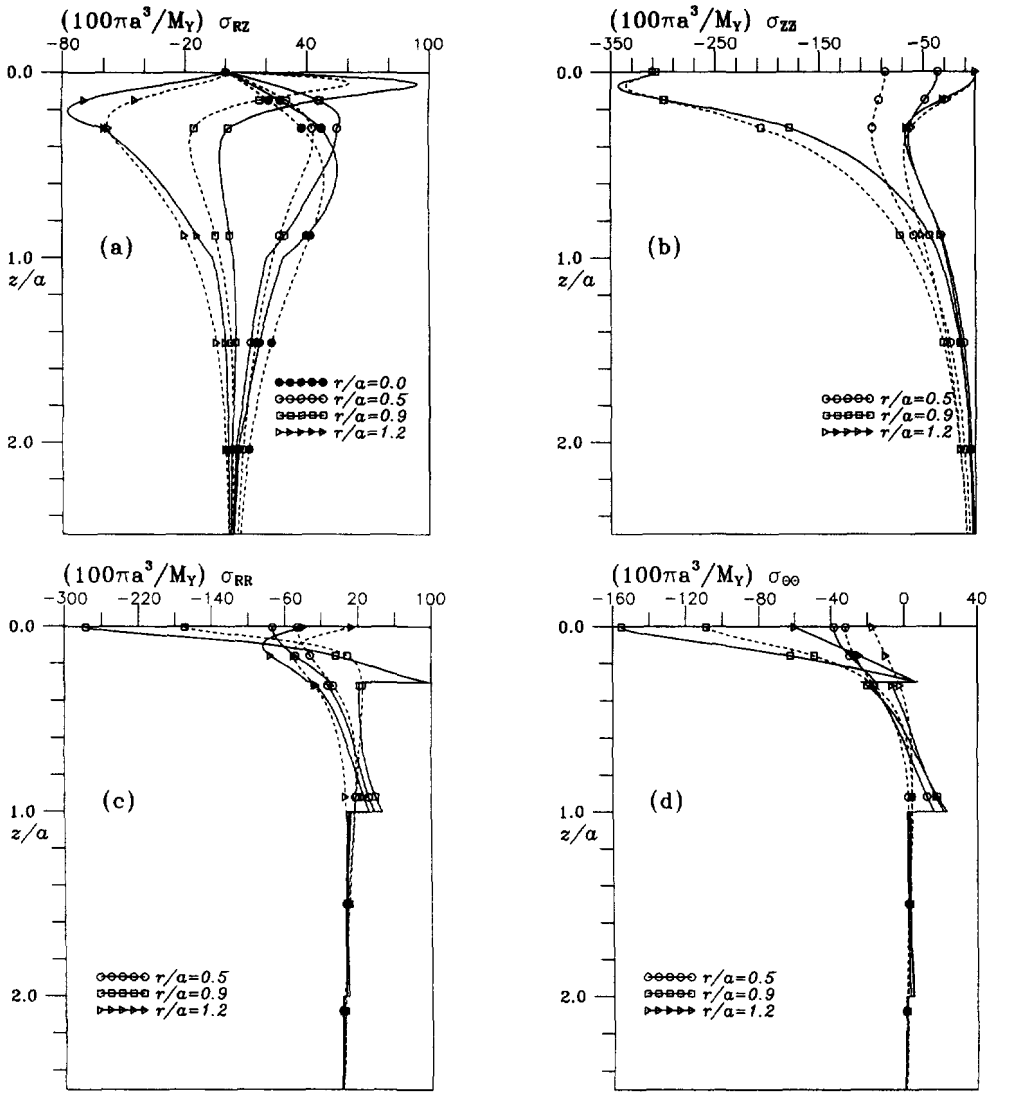

Fig. 11. Stresses vs depth for either a five-layered halfspace (solid line) or a homogeneous halfspace (dashed line) rotationally indented by a rigid plate.

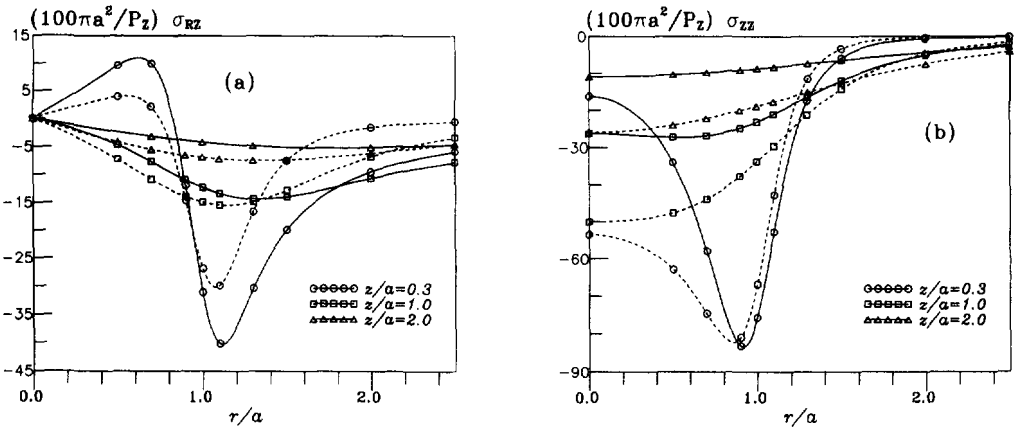

Fig. 12. Vertical stresses vs radial distance for either a five-layered halfspace (solid line) or a homogeneous halfspace (dashed line) axisymmetrically indented by a rigid plate.

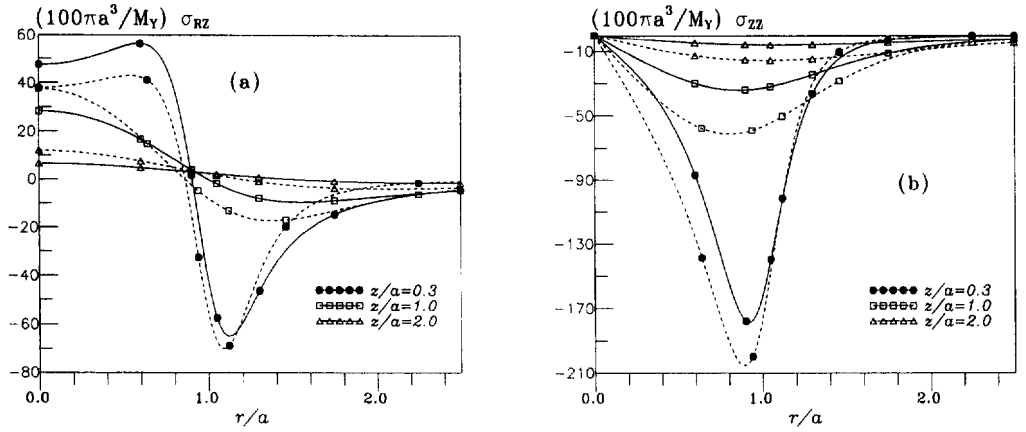

Fig. 13. Vertical stresses vs radial distance for either a five-layered halfspace (solid line) or a homogeneous halfspace (dashed line) rotationally indented by a rigid plate.

halfspaces. The tensile normal stresses at the bottom of an elastic layer (i.e., $z/a = 0.3^-$, 1.0^-, 2.0^-, 3.0^- or 4.3^-) are much higher than those at the top of an elastic layer (i.e., $z/a = 0.3^+$, 1.0^+, 2.0^-, 3.0^+ or 4.3^+) and those at the same depth in the homogeneous elastic halfspace.

12. CONCLUSIONS AND RECOMMENDATIONS

According to the results presented above, one can summarize the conclusions and recommendations as follows.

1. Using classical theory of Fourier integral transforms and the transfer matrix technique, the paper has presented an analytical solution, in the framework of classical elasticity, for the elastic field in a multilayered elastic solid whose surface is subjected to the eccentric indentation of a rigid circular plate.
2. The stress singularity at the edge of the rigid plate in the multilayered elastic solids has been given in exactly closed-form. The direction of crack initiation at the rigid plate edge is affected only by the Poisson's ratio of the top layer near the surface according to a criterion based on the strain energy density factor.
3. The solution has been analytically reduced to the case of a homogeneous elastic halfspace eccentrically indented by a rigid plate. The solution of this special case is presented in the forms of elementary functions.
4. A computational program in FORTRAN has been developed to calculate the displacements, stresses, and strains in the multilayered elastic system induced by the rigid plate. The difficulty associated with the slow convergence of numerical integration near or at the surface of the multilayered solid has been overcome by using an asymptotic technique. In particular, the singularity of the solution at the edge of the rigid plate has been isolated and can be examined analytically and accurately.
5. Numerical verification has been given on the techniques adopted in the paper. It has been shown that the solution is amenable to numerical results with very high efficiency and accuracy.
6. The presented numerical results illustrate that the layering material non-homogeneity has a significant influence on the elastic field induced by the eccentrically loaded rigid plate.
7. Although the paper considers only the perfectly bonded interface condition between any two connected elastic layers, the solution expressions can be directly applied to other interface conditions such as smooth and frictional interface conditions. For the other interface conditions, only the kernel functions (Φ_{13}, Φ_{33}, Ψ_{13} and Ψ_{33}, (15))

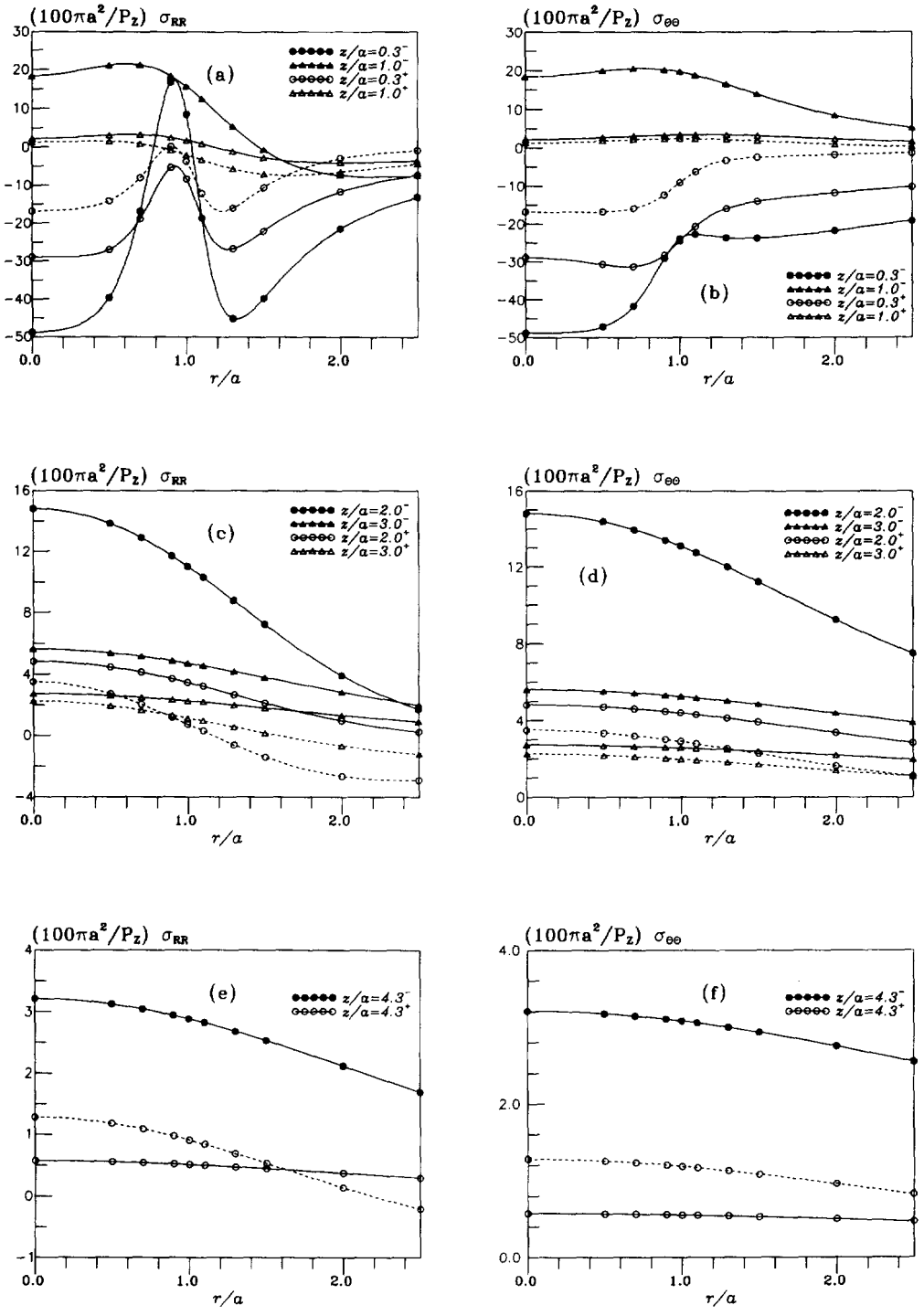

Fig. 14. Horizontal normal stresses vs radial distance for either a five-layered halfspace (solid line) or a homogeneous halfspace (dashed line) axisymmetrically indented by a rigid plate.

need to be re-formulated algebraically using the governing eqns (8)–(11) in the transform domain and the specifically imposed interface conditions.

8. Finally, it is recommended that the analytical solution can be applied to the improvement of the current backcalculation methods associated with the FWD nondestructive testing of highway and airport pavements.

Acknowledgements—The author thanks the referees for their constructive comments and suggestions which enhanced the presentation of this paper.

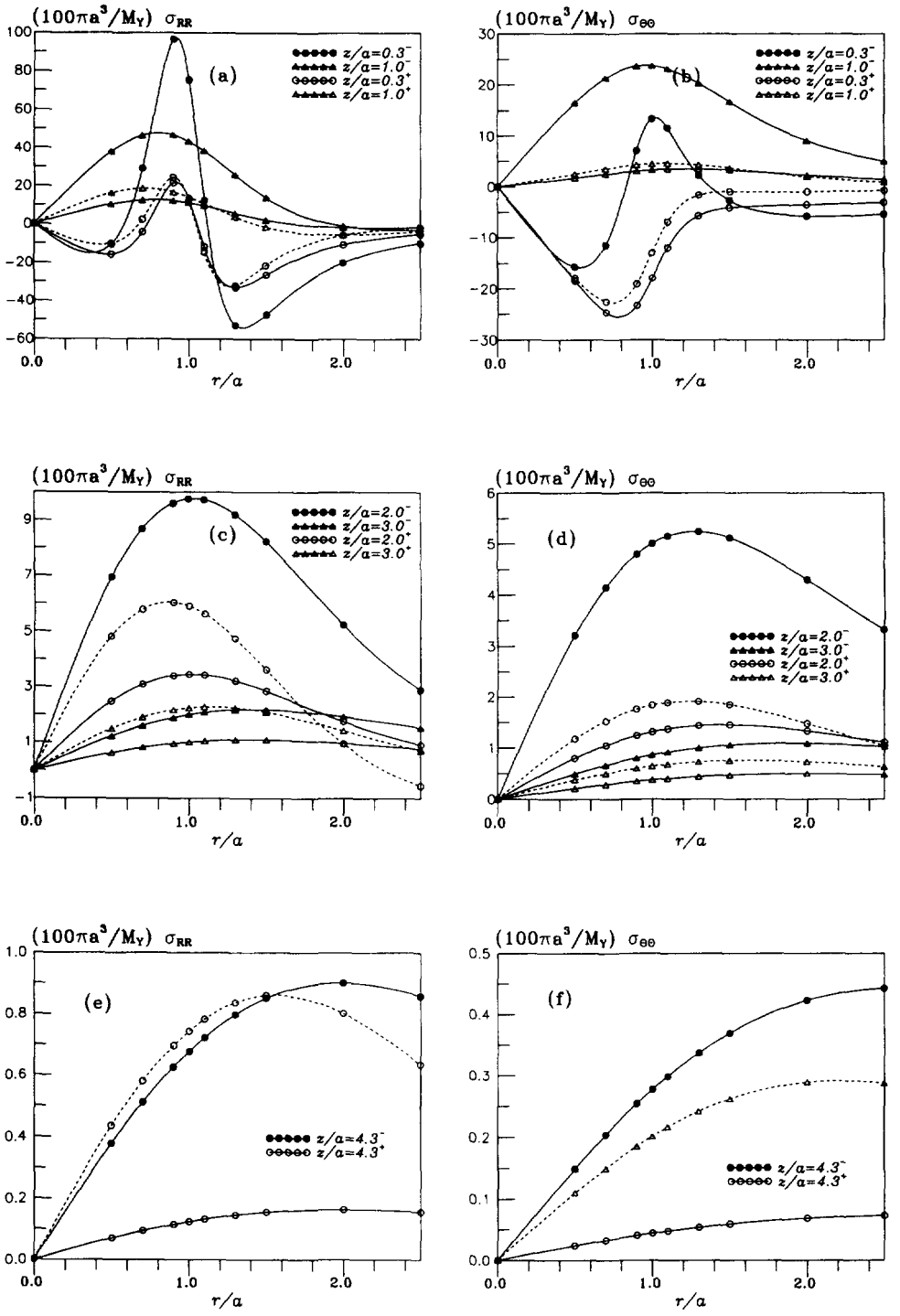

Fig. 15. Horizontal normal stresses vs radial distance for either a five-layered halfspace (solid line) or a homogeneous halfspace (dashed line) rotationally indented by a rigid plate.

REFERENCES

Atkinson, K. (1976). *A Survey of Numerical Methods for the Solution of Fredholm Integral Equations of the Second-Kind*, Soc. Industrial and Appl. Math., Philadelphia, PA.

Baker, C. T. H. (1977). *The Numerical Treatment of Integral Equations*, Clarendon Press, Oxford.

Boddapati, K. M. and Nazarian, S. (1994). Effects of pavement-falling weight deflectometer interaction on measured pavement response. *Non-destructive Testing of Pavements and Backcalculation of Moduli (Second Volume)*, ASTM STP 1198 (eds H. L. V. Quintas, A. J. Bush, and G. Y. Valadi), American Society for Testing and Materials, Philadelphia, pp. 326–342.

Booker, J. R., Balaam, N. P. and Davis, E. H. (1985). The behaviour of an elastic non-homogeneous halfspace. Part II—circular and strip footings. *Int. J. Num. Anal. Methods Geomech.* **9,** 369–381.

Boussinesq, J. (1885). *Applications des potentials à l'étude de l'équilibre et du mouvment des solids élastiques*, Gaythier-Villars, Paris.

Burminster, D. M. (1945). The general theory of stresses and displacements in layered systems I, II, III. *J. Appl. Phys.* **16,** 89–93, 126–127, 296–302.

Bush, A. J. and Baladi, G. Y. eds. (1989). *Non-destructive Testing of Pavements and Backcalculation of Moduli*, ASTM STP 1026, American Society for Testing and Materials, Philadelphia.

Carrier, W. D. and Christian, J. T. (1973). Rigid circular plate resting on a non-homogeneous elastic halfspace. *Geotech.* **23,** 67–84.

Chen, W. T. and Engel, P. A. (1972). Impact and contact stress analysis in multilayer media. *Int. J. Solids Structures* **8,** 1257–1281.

Chow, Y. K. (1987). Vertical deformation of rigid foundations of arbitrary shape on layered soil media. *Int. J. Num. Anal. Methods Geomech.* **11,** 1–15.

Delves, L. M. and Mohamed, J. L. (1985). *Computational Methods for Integral Equations*, Cambridge University Press, Cambridge.

de Pater, A. P. and Kalker, J. J. (1975). *The Mechanics of the Contact Between Deformable Bodies*, Delft University Press, Belgium.

Dhaliwal, R. (1970). Punch problem for an elastic layer overlayering an elastic foundation. *Int. J. Engng Sci.* **8,** 273–288.

Fabrikant, V. I. (1989). *Applications of Potential Theory in Mechanics: A Selection of New Results*, Kluwer Academic Publishers, The Netherlands.

Gao, H., Chiu, C. H., and Lee, J. (1992). Elastic contact versus indentation modeling of multi-layered materials. *Int. J. Solids Structures* **29,** 2471–2492.

Gladwell, G. M. L. (1980). *Contact Problems in the Theory of Elasticity*. Sijthoff and Noordhoff, The Netherlands.

Harding, J. W. and Sneddon, I. N. (1945). The elastic stress produced by the indentation of the plane surface of a semi-infinite elastic solid by a rigid punch. *Proc. Camb. Phil. Soc.* **41,** 16–26.

King, R. B. (1987). Elastic analysis of some punch problems for a layered medium. *Int. J. Solids Structures* **23,** 1657–1664.

Mahoney, J. P., Coetzee, N. F., Stubstad, R. N., and Lee, S. W. (1989). A performance comparison of selected backcalculation computer programs. *Nondestructive Testing of Pavements and Backcalculation of Moduli*, ASTM STP 1026 (eds A. J. Bush and G. Y. Baladi), American Society for Testing and Materials, Philadelphia, pp. 452–467.

May, R. W. and Quintus, H. V. (1994). The quest for a standard guide to NDT backcalculation. *Non-destructive Testing of Pavements and Backcalculation of Moduli (Second Volume)*, ASTM STP 1198 (eds H. L. V. Quintas, A. J. Bush, and G. Y. Baladi), American Society for Testing and Materials, Philadelphia, pp. 505–520.

Monismith, C. L. (1992). Analytically based asphalt pavement design and rehabilitation: Theory to practice. Transportation Research Record 1354, TRB, National Research Council, Washington, D.C., pp. 5–26.

Poulos, H. G. and Davis, E. H. (1974). *Elastic Solutions for Soil and Rock Mechanics*. John Wiley & Sons, Inc., New York.

Rajapakse, R. K. N. D. and Selvadurai, A. P. S. (1991). Response of circular footings and anchor plates in non-homogeneous elastic soils. *Int. J. Num. Anal. Methods Geomech.* **15,** 457–470.

Rowe, R. K. and Booker, J. R. (1981). The behaviour of footings resting on a non-homogeneous soil mass with a crust. Part II. Circular footings. *Can. Geotech. J.* **18,** 265–279.

Schiffman, R. L. (1962). General analysis of stresses and displacements in layered elastic system. *Proc. of Int. Conf. on the Structural Design of Asphalt Pavements*, University of Michigan, Ann Arbor, Michigan, U.S.A., August, pp. 369–384.

Selvadurai, A. P. S. (1979). *Elastic Analysis of Soil Structure Interaction, Developments in Geotechnical Engineering*. Vol. 17, Elsevier, Amsterdam.

Selvadurai, A. P. S. and Yue, Z. Q. (1994). On the indentation of a poroelastic layer. *Int. J. Num. Anal. Methods Geomech.* **18,** 161–175.

Sih, G. C. (1991). *Mechanics of Fracture Initiation and Propagation: Surface and Volume Energy Density Applied as Failure Criterion*, Kluwer Academic Publishers, London.

Sneddon, I. N. (1946). Boussinesq's problem for a flat-ended cylinder. *Proc. Cambridge Philosophical Society* **42,** 29–29.

Sneddon, I. N. (1972). *The Use of Integral Transform*. McGram-Hill Company, New York.

Uflyand, S. (1968). *Integral Transforms in Elasticity Theory*, 2nd edition. Leningrad Izdatelstvo; English translation of the 1st edition, translated W. J. A. White (ed. I. N. Sneddon), North Carolina State University (1995).

Wu, T. S. and Chiu, Y. P. (1967). On the contact problem of layered elastic bodies. *Q. Appl. Math.* **25,** 233–242.

Yue, Z. Q. (1988). Solution for the thermoelastic problem in vertically inhomogeneous media, *Acta Mechanica Sinica*, English edition **4,** 182–189.

Yue, Z. Q. (1992). Mechanics of rigid disc inclusions in fluids saturated poroelastic media, Ph.D. Thesis, Carleton University, Ottawa, Canada.

Yue, Z. Q. (1996). On elastostatics of multilayered solids subjected to general surface traction. *Q. J. Appl. Math. Mech.* **49,** part 3.

Yue, Z. Q. and Selvadurai, A. P. S. (1994). On the asymmetric indentation of a consolidating poroelastic halfspace. *Appl. Math. Modelling* **18,** 171–185.
Yue, Z. Q. and Wang, R. (1988). Static solution for transversely isotropic elastic N-layered systems. *Acta Scientiarum Naturalium. Universitatis Pekinensis* **24,** 202–211 (in Chinese).

APPENDIX A

This appendix contains the closed-form results for the semi-infinite integral with depending parameters defined by the following equations.

$$S_m(t,s,\zeta,k)=\int_0^{\infty}\sin(\rho t)J_m(\rho s)\,e^{-\rho\zeta}\rho^k\,d\rho$$

$$C_m(t,s,\zeta,k)=\int_0^{\infty}\cos(\rho t)J_m(\rho s)\,e^{-\rho\zeta}\rho^k\,d\rho \tag{A1}$$

where $\zeta\geqslant 0$; for S_0, $k=-1,0,1,2,3$; for S_1, $k=-2,-1,0,1,2,3$; for S_2, $k=-2,-1,0,1,2,3$; for S_3, $k=-1,0,1,2,3$; for C_0, $k=0,1,2,3$; for C_1, $k=0,1,2,3$; and for C_2, $k=1,2,3$. It can be shown that these semi-infinite integral can be analytically integrated in the forms of elementary functions as follows.

$$S_0(t,s,\zeta,-1)=\arcsin\left(\frac{2t}{\sqrt{(s+t)^2+\zeta^2}+\sqrt{(s-t)^2+\zeta^2}}\right)$$

$$S_1(t,s,\zeta,-2)=\frac{1}{2s\eta}\left[t(\eta-\zeta)^2+\eta s^2\arctan\left(\frac{t}{\eta}\right)\right]$$

$$S_2(t,s,\zeta,-2)=\frac{t(\zeta-\eta)}{12\eta^3s^2}\left[(\eta-\zeta)^2(t^2-3\eta^2)-3\eta^2s^2\right]$$

$$S_m(t,s,\zeta,k)=-\frac{\partial S_m(t,s,\zeta,k-1)}{\partial\zeta}$$

$$S_2(t,s,\zeta,k)=\frac{2}{s}S_1(t,s,\zeta,k-1)-S_0(t,s,\zeta,k)$$

$$S_3(t,s,\zeta,k)=\frac{4}{s}S_2(t,s,\zeta,k-1)-S_1(t,s,\zeta,k)$$

$$C_m(t,s,\zeta,0)=\frac{\partial S_m(t,s,\zeta,-1)}{\partial t}$$

$$C_m(t,s,\zeta,k)=-\frac{\partial C_m(t,s,\zeta,k-1)}{\partial\zeta}$$

$$C_2(t,s,\zeta,k)=\frac{2}{s}C_1(t,s,\zeta,k-1)-C_0(t,s,\zeta,k) \tag{A2}$$

where $m=0,1$;

$$\eta=\frac{\sqrt{2}}{2}\sqrt{s^2+\zeta^2-t^2+\sqrt{(s^2+\zeta^2-t^2)^2+4t^2\zeta^2}};$$

for S_0, $k\geqslant 0$; for S_1, $k\geqslant -1$; for S_2, $k\geqslant -1$; for S_3, $k\geqslant 0$; for C_j $(j=0,1,2)$, $k\geqslant 1$.

In particular, the elementary functions in eqns (43) are given by the following equations.

$$Z_{mk}=S_m(1,s,\zeta,k-1),\quad k\geqslant 0$$

$$Y_{00}=1-\zeta S_0(1,s,\zeta,-1)-sS_1(1,s,\zeta,-1)$$

$$Y_{0k}=S_0(1,s,\zeta,k-1)-C_0(1,s,\zeta,k),\quad k\geqslant 1$$

$$Y_{10}=sS_0(1,s,\zeta,-1)-\zeta S_1(1,s,\zeta,-1)-S_1(1,s,\zeta,-2)$$

$$Y_{1k}=S_1(1,s,\zeta,k-1)-C_0(1,s,\zeta,k),\quad k\geqslant 1$$

$$Y_{20}=sS_1(1,s,\zeta,-1)+\zeta S_0(1,s,\zeta,-1)-\frac{2\zeta}{s}S_1(1,s,\zeta,-2)-2S_2(1,s,\zeta,-2)$$

$$Y_{21}=sS_1(1,s,\zeta,0)-\zeta S_2(1,s,\zeta,0)+S_0(1,s,\zeta,-1)-\frac{2}{s}S_1(1,s,\zeta,-2)$$

$$Y_{2k}=S_2(1,s,\zeta,k-1)-C_1(1,s,\zeta,k),\quad k\geqslant 2$$

$$Y_{31} = \frac{4}{s} Y_{20} - Y_{11}$$

$$Y_{32} = \frac{4}{s} Y_{21} - Y_{12} \tag{A3}$$

where Z_{mk} and Y_{mk} are defined by

$$Z_{mk} = \int_0^\infty \rho^k e^{-\rho\zeta} J_m(\rho s) \frac{\sin(\rho)}{\rho} d\rho$$

$$Y_{mk} = \int_0^\infty \rho^k e^{-\rho\zeta} J_m(\rho s) \frac{\sin(\rho) - \rho\cos(\rho)}{\rho^2} d\rho. \tag{A4}$$

APPENDIX B

In general, the semi-infinite integrals in the kernel functions (28) and (32) can be evaluated by using the following proceeding limit technique.

$$\int_0^\infty F(\rho)\, d\rho \approx \int_0^{A_0} F(\rho)\, d\rho + \int_{A_0}^{A_1} F(\rho)\, d\rho + \cdots + \int_{A_n}^{A_{n+1}} F(\rho)\, d\rho \tag{B1}$$

where $0 < A_0 < A_1 \cdots < A_{n+1}$ is a sequence of numbers that approaches infinity and the integrand $F(\rho)$ is given in eqns (28), (31), (32), and (34).

Each finite integral on the right-hand side in equation (B1) is proper and can be calculated by using the Simpson's quadrature based adaptively iterative integration. The evaluation of these proceeding finite integrals is automatically terminated provided the following condition is satisfied,

$$\left| \int_{A_n}^{A_{n+1}} F(\rho)\, d\rho \right| \left[1 + \left| \int_{A_0}^{A_{n+1}} F(\rho)\, d\rho \right| \right] \leqslant \varepsilon_a \tag{B2}$$

where ε_a is an assigned absolute or relative error.

If the evaluation depth is near the surface of the multilayered elastic solid, i.e., $0 \leqslant \zeta < H_1/a$, the functions Φ_{13}, Φ_{33}, Ψ_{13}, and Ψ_{33} have the asymptotic functions in the following as ρ is large.

$$\Phi_{13} \approx \tfrac{1}{2}[2\nu_1 - 1 + \rho\zeta] e^{-\rho\zeta}$$

$$\Phi_{33} \approx \tfrac{1}{2}[2(\nu_1 - 1) - \rho\zeta] e^{-\rho\zeta}$$

$$\Psi_{13} \approx -\rho z\, e^{-\rho\zeta}$$

$$\Psi_{33} \approx [1 + \rho z] e^{-\rho\zeta}. \tag{B3}$$

The semi-infinite integrals in eqns (32) associated with the asymptotic functions (B3) can be integrated in exact-closed form by using equations (A2). As a result, the semi-infinite integrals associated with the remaining term in equations (B1) can be evaluated with high accuracy and efficiency. The above procedure can accommodate the problems associated with the semi-infinite integrals with depending parameters.